ANALYSIS OF EFFECTIVE THERMAL CONDUCTIVITY OF FIBROUS MATERIALS

FINAL REPORT

for

NASA Grant NAG 9-532
UH Budget 1-5-54281

by

Michael W. Futschik
Graduate Assistant

Larry C. Witte
Principal Investigator
Professor and Chairman

Department of Mechanical Engineering
University of Houston
Houston, TX
77204-4792

July 1, 1993

Abstract

The objective of this research is to gain a better understanding of the various mechanisms of heat transfer through fibrous materials and to gain insight into how fill-gas pressure influences the effective thermal conductivity. By way of first principles and some empiricism, two mathematical models are constructed to correlate experimental data. The data are obtained from a test series measuring the effective thermal conductivity of Nomex® using a two-sided guarded hot-plate heater apparatus. Tests are conducted for certain mean temperatures and fill-gases over a range of pressures varying from vacuum to atmospheric conditions. The models are then evaluated to determine their effectiveness in representing the effective thermal conductivity of a fibrous material.

The models presented herein predict the effective thermal conductivity of Nomex extremely well. Since the influence of gas conduction is determined to be the most influential component in predicting the effective thermal conductivity of a fibrous material, an improved representation of gas conduction is developed. Finally, some recommendations for extension to other random-oriented fiber materials are made concerning the usefulness of each model depending on their advantages and disadvantages.

TABLE OF CONTENTS

LIST OF TABLES

LIST OF FIGURES

Nomenclature

a = Knudsen accommodation coefficient (-)

b, c = proportionality constant (-)

A = area (m^2)

A_o = approximate overlapping area at fiber contact (m^2)

c_v = specific heat at constant volume (J/kg·°C)

d = thickness of fibrous material (m)

d_{eff} = length of side of rectangular solid of same volume as cylindrical fiber (m)

D = mean diameter of fiber (m)

$\bar{e}$ = average heat energy (J)

E = constant dependent on gas (N/m·°C)

E_i = energy transferred to boundary surface by incident molecules (J)

E_r = energy carried away from the boundary after the incident molecule has rebounded (J)

E_w = energy of rebounded molecules required to be in equilibrium at the boundary temperature (J)

f = Maxwellian velocity distribution (s^3/m^6)

G = temperature jump length (m)

k = Boltzmann constant (J/°C)

K = correction factor for CO_2 thermal conductivity (-)

$\tilde{K}_e$ = Rosseland extinction coefficient (1/m)

l_{eff} = effective conduction path length through fiber (m)

l_d = base length of unit cell (m)

l_o = height of unit cell (m)

m = mass (kg)

M = molecular weight of gas (kg/mole)

n = molecular number density (molecules/m^3)

$\bar{n}$ = normalized number density (-)

N_A = Avagadro's number (molecules/mole)

p = pressure (Pa)

q = heat flux (W/m^2)

Q = heat flow (W)

R = gas constant ($J/kg \cdot °C$)

R_G = thermal resistance of gas per unit area (°C/W)

R_S = thermal resistance of solid phase per unit area (°C/W)

T = temperature (°C or K)

T_c = cold-side temperature (K)

T_h = hot-side temperature (K)

T_m = mean temperature (K)

$\bar{T}$ = normalized temperature (-)

ΔT = temperature difference (°C or K)

u = specific internal energy (J/m)

v = molecule vector velocity (m/s)

$\bar{v}$ = mean velocity of molecule (m/s)

$\bar{y}$ = normalized distance between parallel plates (-)

Greek Symbols

γ = specific heat ratio (-)

δ = molecular diameter (m)

ε = porosity of fibrous material (-)

$\varepsilon_P, \varepsilon_S, \alpha$ = structural parameters of fibrous material (-)

κ = proportionality constant of inverse fifth power law (Nm^5/kg^2)

κ' = proportionality constant (-)

ϕ = the angle of inclination between the diagonal of unit cell base and y-axis (rad)

λ = effective (apparent) thermal conductivity ($W/m \cdot °C$)

λ_{exp} = experimentally measured effective thermal conductivity ($W/m \cdot °C$)

λ_g = thermal conductivity of gas ($W/m \cdot °C$)

$\lambda_{g\ red}$ = thermal conductivity of gas at reduced pressure in fibrous material ($W/m \cdot °C$)

$\lambda_{g\ ref}$ = thermal conductivity of gas at reference temperature, ambient pressure ($W/m \cdot °C$)

λ_h = effective thermal conductivity of horizontal unit cell ($W/m \cdot °C$)

λ_s = thermal conductivity of solid phase (fibers) ($W/m \cdot °C$)

λ_G = effective thermal conductivity due to conduction in gas ($W/m \cdot °C$)

λ_F = effective thermal conductivity due to conduction in fibers and fiber contacts ($W/m \cdot °C$)

λ_R = effective thermal conductivity due to the influence of radiation ($W/m \cdot °C$)

λ_v = effective thermal conductivity of vertical unit cell ($W/m \cdot °C$)

λ_{vac} = effective thermal conductivity at vacuum ($W/m \cdot °C$)

Λ = mean free path of molecule (m)

Λ_o = mean free path of rarefied gas based on length scale of gas enclosure (m)

ρ = density (kg/m^3)

ρ_o = maximum density of fibrous material obtained at which fracture of fibers is imminent (kg/m^3)

ρ_s = density of solid fiber (kg/m^3)

σ = Stefan-Boltzmann constant ($W/m^2 \cdot K^4$)

σ_c = collision cross-sectional area (m^2)

Σ = emissivity of fibers (-)

Σ_o = emissivity of boundary surfaces (-)

Σ_T = total effective emissivity (-)

θ = angle at which two fibers overlap (rad)

θ_c = critical angle below which the overlapped area is no longer rhombus in shape (rad)

Θ = moment of Maxwellian distribution function of Θ (-)

$\langle\Theta\rangle$ = mean quantity averaged over the entire velocity space (-)

Chapter 1 *Introduction*

Insulation materials are used abundantly for space-related applications. These materials may be subjected to harsh conditions that vary from the hot vacuum conditions during a lunar day to the frigid vacuum conditions of a lunar night; from the low-pressure CO_2 environment of Mars to the enormously high temperatures and pressures encountered on the surface of a spacecraft upon reentry. The thermal performance of fibrous materials is of critical importance for the protection of software, hardware equipment, fluid systems, and most of all, human life. Since these materials may be employed for the insulation of habitat modules, space suits, and advanced spacecraft, it is important to understand the heat transfer mechanisms that influence design optimization and safety.

Nomex® is chosen as the test specimen due to its popularity in space-related applications and for its potential for more advanced space applications. Nomex is an aramid filament yarn manufactured by DuPont® and assembled into bats, or blankets, by several other companies. Nomex comes in the form of felt or twill depending on the method of compiling the fibers into a blanket. Of particular interest is the Nomex felt since it is comprised of randomly oriented fibers. Due to its high insulating properties, flame retardance, strength, and tenacity, Nomex has been used in flight jackets, firefighter garments, astronaut suits, space shuttle tiles, and many other applications. Since this is a candidate material for so many space-related applications, its thermal performance is investigated under some various environmental scenarios (different fill-gases and various pressures) and analyzed in an attempt to better understand the various mechanisms of heat transfer involved. In this way, with a better understanding of how heat is transferred through fibrous materials, an accurate model can be developed to predict the thermal performance of a fibrous material.

Heat transfer through fibrous materials is often encountered in engineering practice and is therefore of considerable importance. Some approaches to the study of heat transfer through fibrous materials at reduced fill-gas pressures have been offered; however, difficulties in modeling techniques arise due to the limitations in the ability to represent the physical structure of the fibrous material. The understanding of energy transfer through rarefied gases is also limited. This limitation can cripple the accuracy of models that predict the effective thermal conductivity of these materials in low pressure environments.

The objective of this research is to gain a better understanding of the effects of various fill-gas pressures on the effective thermal conductivity of certain insulating materials being considered for space-related applications. A set of experiments are conducted involving a specimen tested at various temperatures (-50°C to 20°C) and fill-gas pressures ranging from thermal vacuum (~ 10^{-4} Pa) to atmospheric conditions (~101 kPa). The ultimate goal is to analyze the mechanisms of heat transfer through fibrous materials and to develop a mathematical model that correlates these mechanisms.

Various models have been developed to evaluate the thermal conductivity of fibrous materials [1, 2, 3, 4]. Some of these models are investigated and compared to experimental results obtained as a part of this study. The models take into account the structural arrangement of the solid fibers with respect to the direction of the heat flow. Two models in particular are investigated for the solid- and gas-phase conduction component of the overall effective thermal conductivity of a fibrous material. The first model presented is referred to as the SPCM (Series/Parallel Conduction Model) while the second is referred to as the UCCM (Unit Cell Conduction Model). Both of these models use the same representation for the radiation component of heat transfer. The development of these two models is based on studies available in the literature combined with

modifications and corrections developed herein. These models are analyzed for their validity in mathematically representing a real fibrous material and for the accuracy of their effective thermal conductivity predictions when compared to experimental data.

Chapter 2 *Models of Conductive Heat Transfer*

2.1 *Introduction*

The purpose of thermal insulation is to reduce heat flow across temperature differences. There are many thermal insulations available that differ in physical structure depending on the intended application. Closed-cell materials such as cork, Rubatex®, and Styrofoam® are comprised of small vacuoles, or cells. Fibrous materials such as Nomex and Corning Fiberglass® are considered open-pore systems. Insulations such as aluminized Mylar® comprise of multiple layers of a highly reflective material and are effective only in a thermal vacuum where radiation is the principal transport of heat energy. There are many others, but they are all designed for the purpose of reducing the flow of heat.

Closed cell systems are not very useful when subjected to severe pressure changes. The air within the cell (or other gas residing within the void) will expand deforming the material and typically rupturing the cell as the pressure decreases. If the material is then brought back to ambient conditions, the material tends to collapse to smaller dimensions than those of its original configuration. With the cells ruptured, its effectiveness as an insulating material is decreased.

Fibrous materials are considered open-pore systems. They not only can be used for various pressure scenarios, but their thermal performance as an insulation is actually increased as the pressure decreases. This makes fibrous materials extremely useful for space-based applications. Fibrous materials hinder gas flow past a surface thereby reducing the heat transferred by convection. Also, since typical fibrous insulations have a

porosity of 0.9 or greater, the heat transferred purely by conduction through the solid fibers and fiber contact points is small. These characteristics make fibrous insulations very effective.

In fibrous materials, heat is transferred by several modes: conduction through the solid fibers and fiber contact points constituting the insulation, conduction and convection through the gas residing within the voids of the insulation, and radiation within the material. The effective thermal conductivity of a fibrous material, λ, may be expressed as [1, 2]

$$\lambda = \lambda_G + \lambda_F + \lambda_R \,, \tag{1}$$

where λ_G = the effective thermal conductivity due to conduction in the gas,

λ_F = the effective thermal conductivity due to conduction in the solid fibers and fiber contacts, and

λ_R = the effective thermal conductivity due to the influence of radiation within the material.

Two conductivity models will be presented based on previous work with the addition of significant modifications by the present author.

2.2 *Series/Parallel Conduction Model*

The SPCM is illustrated by Figs. 1 and 2. Figure 1 shows the solid phase and gas phase in *series* with one another with respect to the direction of the heat flow. Figure 2 shows the solid and gas phases *parallel* to the direction of the heat flow. It can be shown that the total thermal resistivity for the structure shown in Fig. 1 is simply the sum of the

reciprocals of the individual thermal conductivities of each of the constituent components [1]. The reciprocal of the resulting sum is the effective thermal conductivity. Similarly for Fig. 2, the effective thermal conductivity is the sum of the individual thermal conductivities of each constituent component. Thus, the effective thermal conductivity for the series structure, λ_S, can be expressed as

$$\lambda_S = \frac{\lambda_s \lambda_g}{\varepsilon \lambda_s + (1 - \varepsilon)\lambda_g}, \tag{2}$$

where ε = porosity of the material,

λ_s = the thermal conductivity of the solid fibers, and

λ_g = the thermal conductivity of the gas.

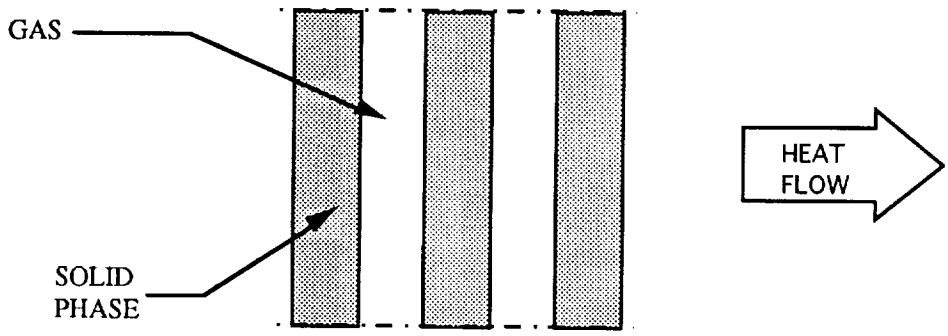

Figure 1. Solid and gas phases in series with respect to the direction of heat flow

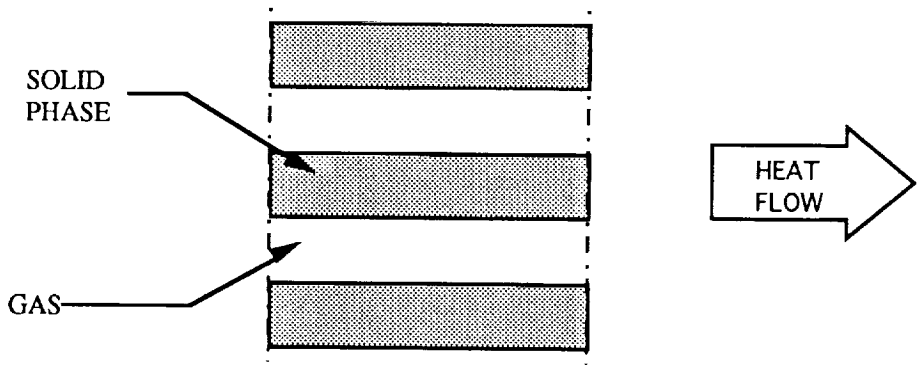

Figure 2. Solid and gas phases in parallel with respect to the direction of heat flow

Similarly for the parallel structure, the effective thermal conductivity, λ_P, can be expressed as

$$\lambda_P = \varepsilon\lambda_g + (1 - \varepsilon)\lambda_s \, . \tag{3}$$

These values, λ_S and λ_P, are extreme cases, and it would be reasonable to assume that the actual effective thermal conductivity of a *real* fibrous material is somewhere between these estimated values. Therefore, it is considered that a fraction of the material is structured in parallel and the remaining fraction is structured in series to the direction of the flow of heat [1]. Neglecting radiation, the effective thermal conductivity of a material structured in this way can be expressed as

$$\lambda = \alpha\left(\varepsilon_P\lambda_g + (1 - \varepsilon_P)\lambda_s\right) + (1 - \alpha)\left(\frac{\lambda_s\lambda_g}{\varepsilon_S\lambda_s + (1 - \varepsilon_S)\lambda_g}\right), \tag{4}$$

where α is the fraction of the material that is structured parallel to the direction of the flow of heat, and ε_S and ε_P are related to the porosity, ε, by

$$\varepsilon = (1 - \alpha)\,\varepsilon_S + \alpha\varepsilon_P \, . \tag{5}$$

2.3 *Unit Cell Conduction Model*

Another model (UCCM) has been proposed that depicts the fibrous material as composed of unit cells oriented randomly throughout the structure [4, 5]. An example of a unit cell model which consists of a cell of dimension l_o by l_o for the base, and l_d as the height is shown in Figure 3. Two semicylindrical bodies representing the solid fibers intersect the top and bottom faces of the cell. Although this model attempts to more accurately model the random positioning of the fibers, it neglects to take into account fiber

contact points. To compensate for this, the fibers of the unit cell have an *effective* thermal conductivity (rather than the true thermal conductivity of the fiber) so that the fiber contacts are indirectly taken into account. The thermal resistance between two fibers in contact can be assumed to be much greater than the resistance to heat flow within the fiber itself. Therefore, contact points between fibers are neglected where the fiber is considered oriented in the direction of the principal temperature gradient. The *apparent* contact points are locations within the structure where, in order for the heat to flow in the direction of the principal temperature gradient, it flows through a contact point from one fiber to another. Therefore, an effective conduction path length, l_{eff}, is defined as the distance along which the heat flows until reaching an apparent contact point [5]. This concept will be further discussed in Section 2.3.1.

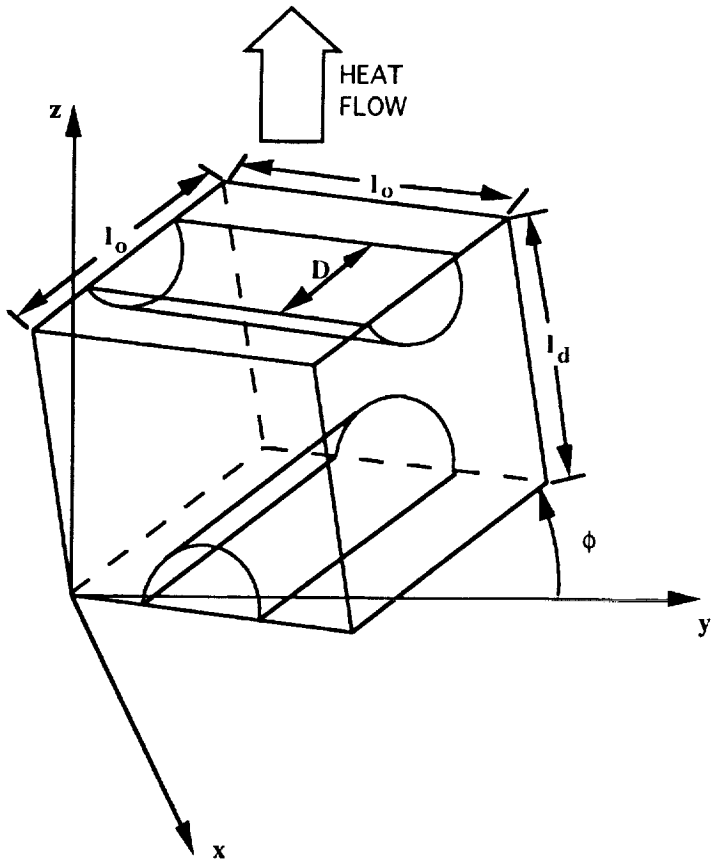

Figure 3. Unit cell model of the structure of a fibrous material

The effective thermal conductivity, λ, of a unit cell oriented in some random position with respect to the principal direction of heat flow is determined from the fraction of the effective thermal conductivity due to the horizontal unit cell and the remaining fraction due to the vertical cell. Therefore, the effective thermal conductivity of a unit cell randomly oriented can be expressed as

$$\lambda = \lambda_v \sin^2\phi + \lambda_h \cos^2\phi \,, \tag{6}$$

where λ_v = effective thermal conductivity of vertical unit cell,

λ_h = effective thermal conductivity of horizontal unit cell,

ϕ = the angle of inclination between the diagonal of unit cell base and the y-axis,

and the heat transfer is in the direction of the positive z-axis.

The effective thermal conductivity of the unit cell can be calculated analogous to the resistances (or conductances) of an electric circuit. Figure 4(a) depicts an electrical circuit that is analogous to a unit cell oriented horizontally ($\phi = 0$) as shown in Fig. 5. This can be simplified by representing cylindrical fibers by rectangular solids of the same volume as shown in Fig. 5 [5]. If it is defined that

$$d_{eff} = \frac{\sqrt{\pi} D}{2} \,, \tag{7}$$

where D = the diameter of fiber and

d_{eff} = length of side of rectangular solid of same volume as cylindrical fiber,

then the thermal resistance per unit area due to the gas, corresponding to R_{G1} in Fig. 4(a), can be represented by

$$R_{G1} = \frac{d_{eff}/2}{\lambda_g l_o (l_o - d_{eff})} . \quad (8)$$

Similarly, The thermal resistance due to conduction in the solid can be expressed as

$$R_{S1} = \frac{d_{eff}/2}{\lambda_s l_o d_{eff}} . \quad (9)$$

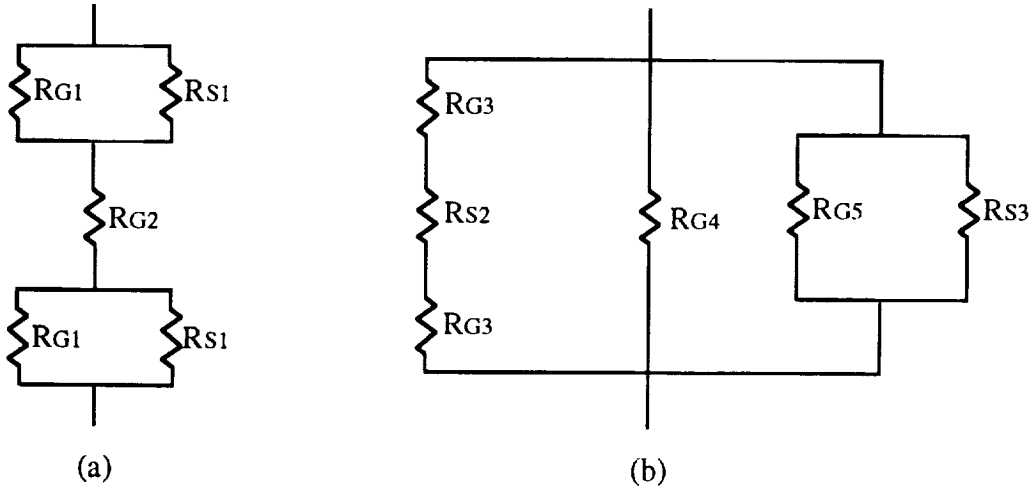

Figure 4. Resistance diagrams analogous to unit cell model (a) unit cell oriented horizontal with respect to heat flow (b) unit cell oriented vertical with respect to heat flow

The thermal resistance, R_{G2}, is due to the horizontal slice of gas between the solid fibers and can be expressed as

$$R_{G2} = \frac{l_d - d_{eff}}{\lambda_g l_o^2} . \quad (10)$$

Then the total effective thermal resistance of a unit cell oriented horizontally with respect to the heat flow is evaluated as

$$R_{tot} = \frac{2R_{G1}R_{S1}}{R_{G1} + R_{S1}} + R_{G2} . \quad (11)$$

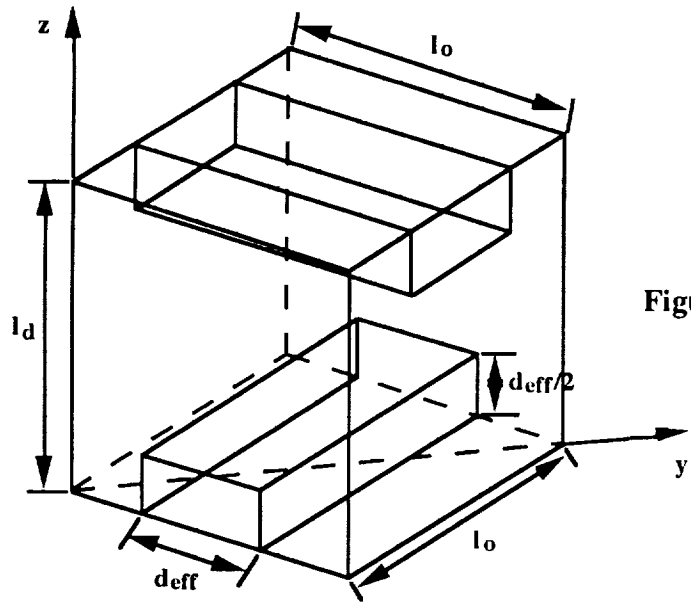

Figure 5. Horizontal unit cell model

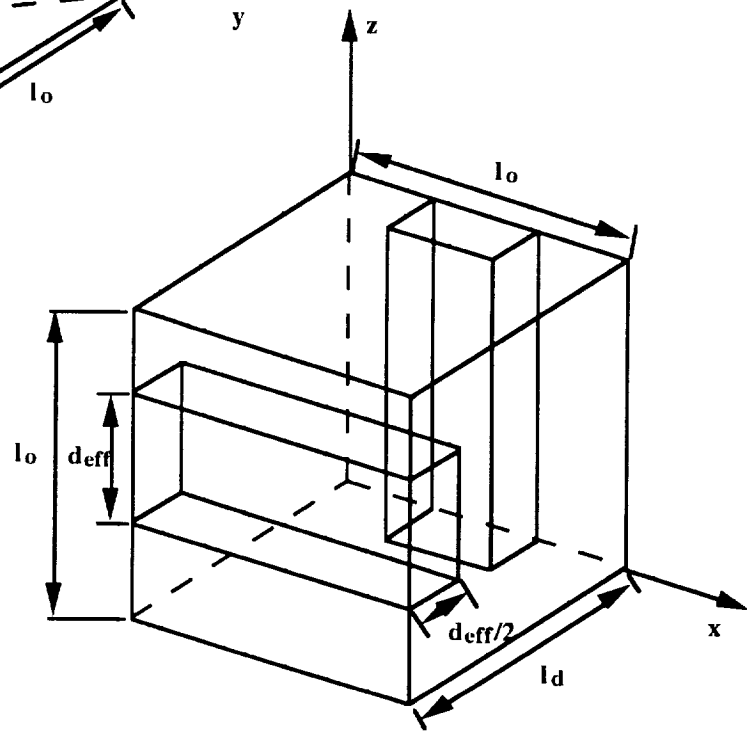

Figure 6. Vertical unit cell model

After some algebraic manipulation, the effective thermal conductivity of a unit cell oriented horizontally with respect to heat flow can be expressed as

$$\lambda_h = \frac{1}{\dfrac{l_o d_{eff}}{\lambda_g l_d (l_o - d_{eff}) + \lambda_s d_{eff} l_d} + \dfrac{(l_d - d_{eff})}{\lambda_g l_d}} \quad . \tag{12}$$

Similarly, the effective thermal conductivity of a unit cell oriented vertically (see Fig. 4(b) and Fig. 6) with respect to the heat flow can be expressed as

$$\lambda_v = \frac{\lambda_g \lambda_s l_o (d_{eff}/2)}{\lambda_s l_d (l_o - d_{eff}) + \lambda_g l_d d_{eff}} + \frac{\lambda_g (l_d - d_{eff})}{l_d} + \frac{\lambda_g (d_{eff}/2)(l_o - d_{eff})}{l_o l_d} + \frac{\lambda_{s,eff} (d_{eff}^2/2)}{l_o l_d} \quad (13)$$

Notice that the last term contains $\lambda_{s,eff}$. This is to indicate that the effective thermal conductivity of the solid fiber is to be used rather than the actual thermal conductivity of the solid. The actual thermal conductivity is used elsewhere where λ_s appears. This substitution is done to compensate for point contacts (as mentioned previously) within the fibrous material. A representation for the effective thermal conductivity of the solid phase, $\lambda_{s,eff}$, was developed by Imakoma et al. [5] and will be derived in the following section.

2.3.1 *Thermal Resistance at Fiber Contact Point*

The resistance representation shown in Fig. 7 assumes that all the heat flux through the fiber is transferred through the thermal resistance at the contact point; that is, the heat transferred through the fiber equals the sum of the heat transferred at the contact point by solid conduction, radiation, and gas conduction. The heat transfer through the solid fiber can be expressed by Fourier's law of conduction,

$$Q = \lambda_{s,eff} \, d_{eff}^2 \frac{(T_1 - T_2)}{(l_{eff}/2)}, \quad (14)$$

where $d_{eff} = \frac{\sqrt{\pi} D}{2}$ and

l_{eff} = effective conduction path length through the fiber.

The effective conduction path length, l_{eff}, is defined as the distance along which the heat flows through a fiber until reaching an apparent contact point. The apparent contact points are locations within the structure where, in order for the heat to continue to transfer in the

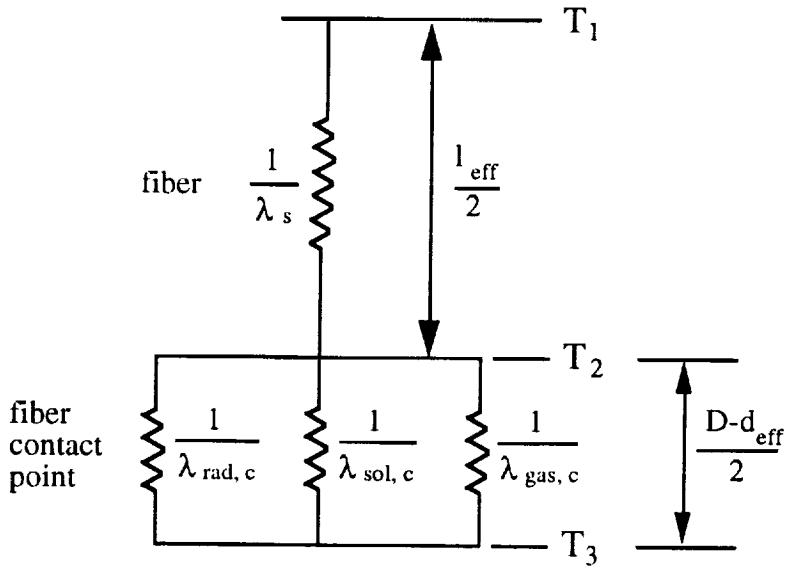

Figure 7. Representation of contact resistance at fiber contact point

principal direction of heat flow, heat actually transfers through a contact point from one fiber to another. All the heat flowing through the fiber according to eqn.(14) is assumed to flow through the apparent contact point. The heat transfer due to radiation at the contact point can be expressed as

$$Q_{rad} = \lambda_{rad,c} 2A_o \frac{(T_2 - T_3)}{D - d_{eff}}, \qquad (15)$$

where A_o = approximate overlapping area at fiber contact and

D = fiber diameter.

Similarly, the heat transferred by gas conduction, Q_{gas}, and by solid conduction, Q_{sol}, are, respectively,

$$Q_{gas} = \lambda_{gas,c} 2A_o \frac{(T_2 - T_3)}{D - d_{eff}} \qquad (16)$$

and

$$Q_{sol} = h_c A_c (T_2 - T_3) , \tag{17}$$

where h_c = heat transfer coefficient at contact point and

A_c = area of contact point.

Since it is assumed that

$$Q = Q_{rad} + Q_{sol} + Q_{gas} , \tag{18}$$

the effective thermal conductivity of solid fibers at a point contact can be expressed as

$$\lambda_{s,eff} = \frac{l_{eff}/2}{d_{eff}^2}\left[\frac{1}{\frac{l_{eff}/2}{\lambda_s d_{eff}^2} + \frac{(D - d_{eff})}{2A_o(\lambda_{gas,c} + \lambda_{rad,c}) + h_c A_c (D - d_{eff})}}\right] . \tag{19}$$

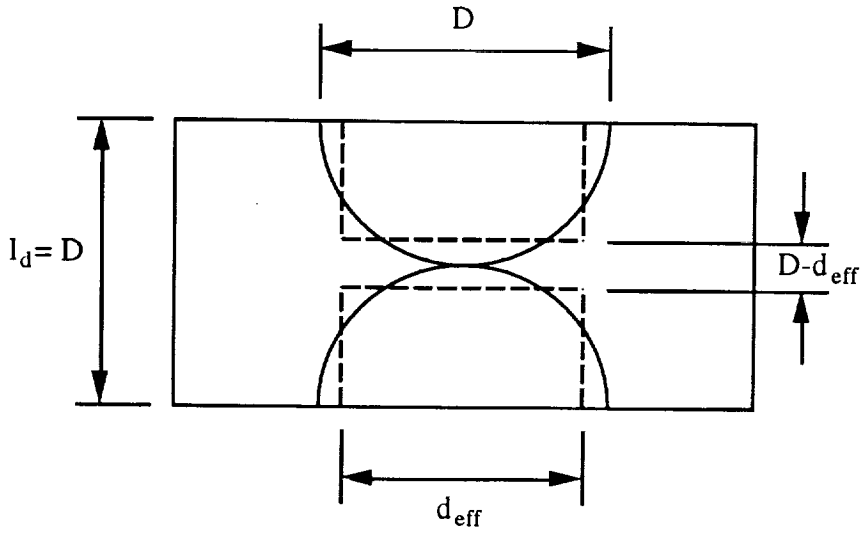

Figure 8. Representation of fiber contact point

If the rectangular solid approximation is used for two fibers in contact, the contact point can be modeled as two parallel plates separated by a distance of D - d_{eff} (see Fig. 8). Therefore, the thermal conductivity due to the gas at the contact point, $\lambda_{gas,c}$, and the

thermal conductivity due to the influence of radiation at the contact point, $\lambda_{rad,c}$, can be expressed, respectively, as

$$\lambda_{gas,c} = \lambda_g \left[1 + \frac{15}{4} \frac{\Lambda}{(D - d_{eff})} \right]^{-1} \tag{20}$$

and

$$\lambda_{rad,c} = 4\sigma (D - d_{eff}) T_m^3 \ . \tag{21}$$

Similar equations will be defined in modeling the conductivity of gas at reduced pressures and the radiative thermal conductivity within a fibrous material; thus, the derivation of eqns.(20) and (21) will become more readily apparent.

2.3.2 *Derivation of Dimensional Parameters for Unit Cell*

Several physical parameters have to be defined for the UCCM in order to evaluate eqns.(12), (13), and (19). The parameters l_o, l_d, and A_o can be represented mathematically and will be derived below.

The porosity, ε, of a fibrous material can be approximated as

$$\varepsilon \cong 1 - \frac{\rho}{\rho_s} \ , \tag{22}$$

where ρ = the density of the fibrous material and

ρ_s = the density of the solid fibers.

Comparison to the unit cell model in Fig. 3 yields

$$\varepsilon = 1 - \frac{\pi D^2/4}{l_o l_d} \cong 1 - \frac{\rho}{\rho_s} \ . \tag{23}$$

Solving for l_o and l_d yields

$$l_o = \frac{\pi D^2}{4} \frac{\rho_s}{l_d \rho} \tag{24}$$

and

$$l_d = \frac{\pi D^2}{4} \frac{\rho_s}{l_o \rho} . \tag{25}$$

If the fibrous material is compressed to its maximum (the point at which the fracture of fibers is imminent), then $l_d = D$ and $\rho = \rho_o$ where ρ_o is the maximum density. Then eqn.(24) can be expressed as

$$l_o = \frac{\pi D}{4} \frac{\rho_s}{\rho_o} . \tag{26}$$

Equations (25) and (26) define the dimensions of the unit cell for the UCCM.

The approximate average area, A_o, overlapped by two fibers in contact modeled as two parallel plates can be evaluated according to Fig. 9a [5]. The range of angles at which the fibers cross is taken to be $0 \le \theta \le \pi/2$. It can be shown that the overlapping area is

$$A_{o1} = \frac{d_{eff}^2}{\sin \theta} , \qquad \theta_c \le \theta \le \frac{\pi}{2} , \tag{27}$$

where θ_c is some critical angle below which the overlapped area is no longer rhombus in shape (see Fig. 9b, c) and is defined as

$$\theta_c = \tan^{-1}\left(\frac{4 d_{eff}}{l_{eff}}\right) . \tag{28}$$

For $0 \le \theta \le \theta_c$, the area can be approximated by subtracting the area shaded in Fig. 9c from the maximum area possible at $\theta = 0$. This assumes that the maximum overlapping length is half the effective conduction path length, $l_{eff}/2$. This yields the second part of the overlapped area, A_{o2}, which can be expressed as

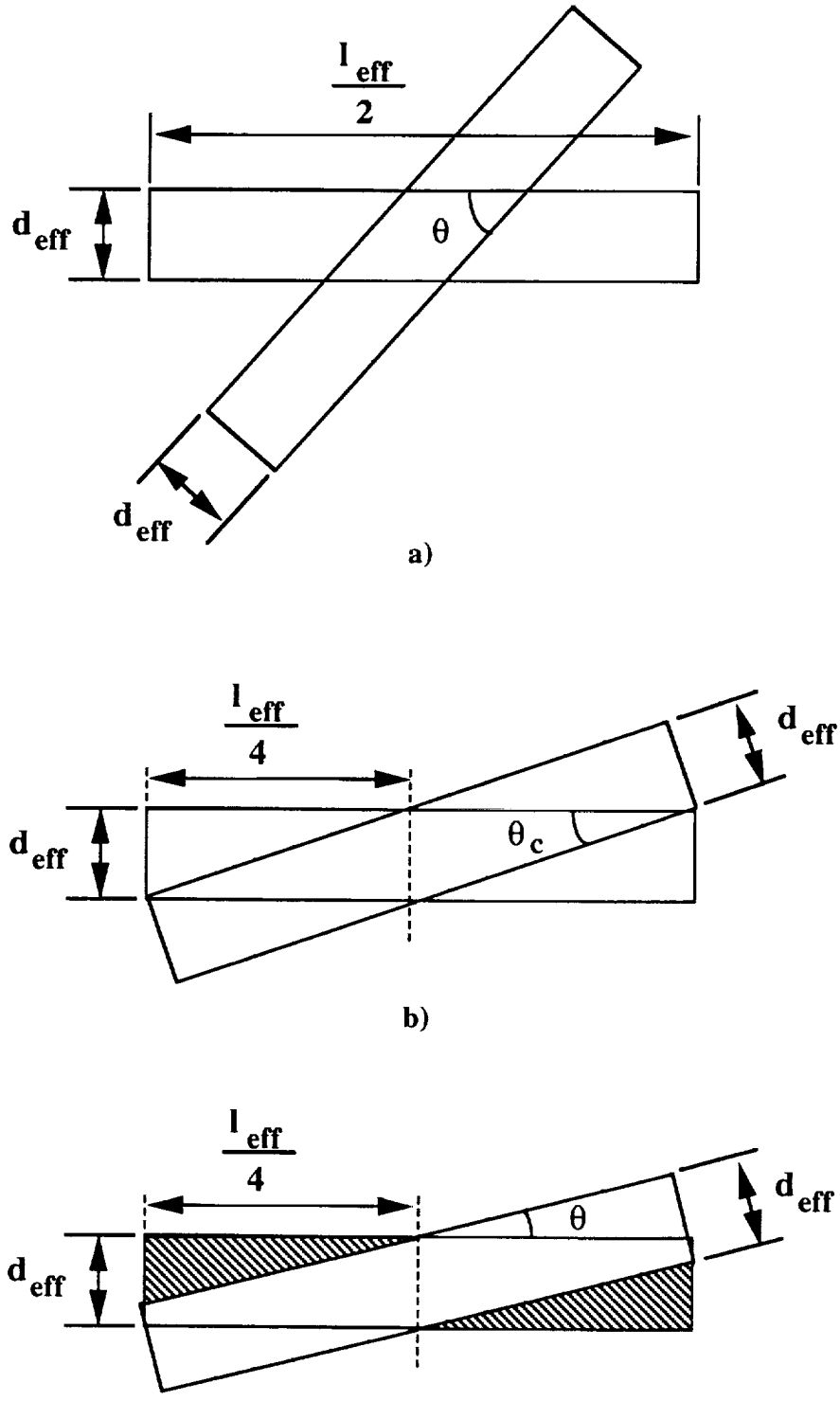

Figure 9. Overlapping area of fibers for various angles of θ

$$A_{o2} = \frac{l_{eff} d_{eff}}{2} - \left(\frac{l_{eff}}{4}\right)^2 \tan\theta \ , \qquad 0 \le \theta \le \theta_c \ . \tag{29}$$

Now, taking the average yields the average overlapping area of the fibers, A_o, which can be expressed as [5]

$$A_o = \frac{\int_{\theta_c}^{\pi/2} A_{o1}\, d\theta + \int_0^{\theta_c} A_{o2}\, d\theta}{\int_0^{\pi/2} d\theta} \ . \tag{30}$$

Substituting the expressions for A_{o1} and A_{o2} yields

$$A_o = \frac{\int_{\theta_c}^{\pi/2} \frac{d_{eff}^2}{\sin\theta}\, d\theta + \int_0^{\theta_c} \left\{\frac{l_{eff} d_{eff}}{2} - \left(\frac{l_{eff}}{4}\right)^2 \tan\theta\right\} d\theta}{\int_0^{\pi/2} d\theta} \ . \tag{31}$$

Evaluating the integrals, the average overlapping area of the parallel plates used to model the cross-over contact between two fibers can be expressed as

$$A_o = \left(\frac{1}{\pi}\right)\left\{\left[-2d_{eff}^2 \ln\left|\tan\left(\frac{\theta_c}{2}\right)\right|\right] + l_{eff} d_{eff} \theta_c - \frac{l_{eff}^2}{8} \ln\left|\sec\theta_c\right|\right\} . \tag{32}^{\dagger}$$

† It seems that there is a discrepancy between eqn.(32) and the equation that Imakoma developed. The present author acknowledges that the approach used in obtaining eqn.(32) was acquired from Imakoma's publication [5]; however, Imakoma obtained a $\sin(\theta_c)$ as the argument of the natural logarithm in the first term. It turns out that since θ_c is small, this difference is negligible.

2.4 *Radiative Conduction Model*

The radiation component of the effective thermal conductivity, λ_R, can be modeled as if the fibers are arranged in planes normal to the direction of heat flow (Fig. 10). The heat flux due to radiation through a material of n fibrous layers can be expressed as

$$q = \frac{\sigma\left(T_h^4 - T_c^4\right)}{2\left(\frac{1}{\Sigma_o} + \frac{1}{\Sigma} - 1\right) + (n-2)\left(\frac{2}{\Sigma} - 1\right)} \tag{33}$$

where σ = Stefan-Boltzman constant,

Σ_o = the emissivity of the wall,

Σ = the emissivity of the fibers, and

n = the number of layers within the fibrous material.

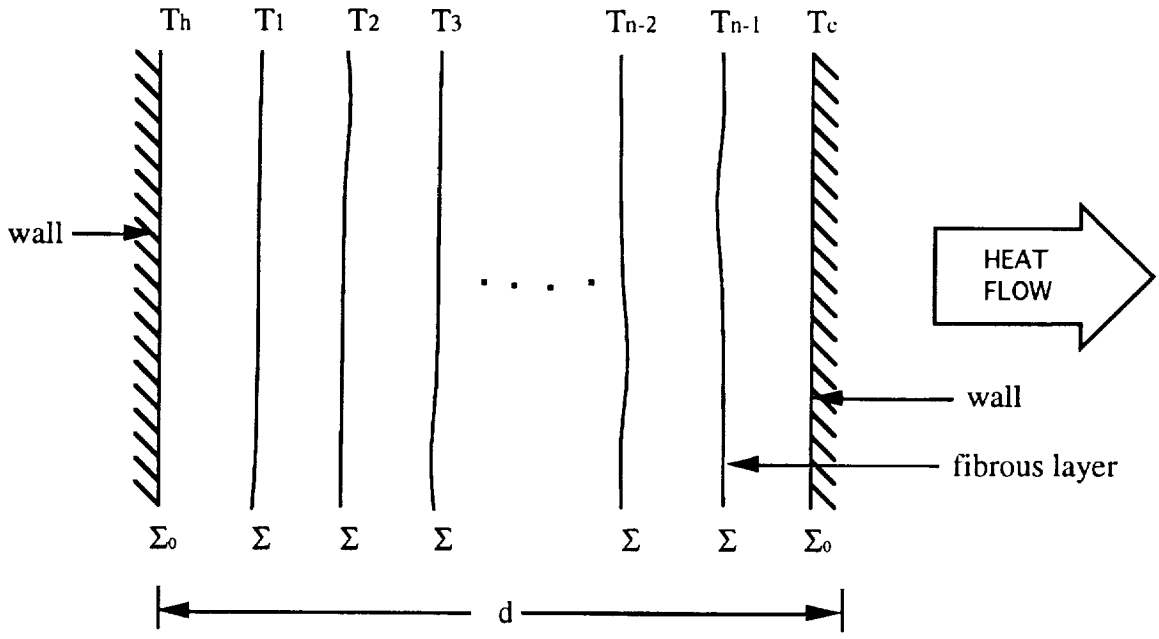

Figure 10. Structure used in modeling radiation heat transfer

Since, from Fourier's Law in one-dimension, the thermal conductivity takes the form of

$$\lambda = \frac{q\,d}{\Delta T} \tag{34}$$

where

q = the heat flux due to radiation given in eqn.(33),

$\Delta T = T_h - T_c$, and

d = the thickness of the fibrous material,

then eqn.(33) can be arranged to take the form of Fourier's Law and appear as a *radiative* conduction equation [6]. The result is an apparent radiative thermal conductivity, λ_R. Allowing the total effective emissivity of a material of *n* layers oriented normal to the direction of the flow of heat to be denoted by Σ_T, it can be expressed as

$$\Sigma_T = \frac{1}{2\left(\frac{1}{\Sigma_o} + \frac{1}{\Sigma} - 1\right) + (n-2)\left(\frac{2}{\Sigma} - 1\right)} \,. \tag{35}$$

Then the radiative component of the thermal conductivity can be expressed as

$$\lambda_R = \sigma \Sigma_T d (T_h + T_c)\left(T_h^2 + T_c^2\right) \,. \tag{36}$$

If the temperature difference, ΔT, is small compared to the magnitude of the absolute temperature, then eqn.(36) can be expressed as [6]

$$\lambda_R = 4\sigma \Sigma_T d\, T_m^3 \,, \tag{37}$$

where T_m is the mean temperature of the fibrous material. This is similar to the model used by Bankvall [1] where $\Sigma_T\, d = \beta \Lambda_o$ and β is called the radiation coefficient. Verschoor and Greebler [3] also derived an expression similar to eqn.(37) where $\Sigma_T\, d = \Lambda_o/\alpha^2$, i.e. $\beta = 1/\alpha^2$ and it is called the opacity factor. Imakoma et al. [4, 5] developed an

expression comparable to eqn.(37) if $\Sigma_T\, d = 4/(3\alpha\rho)$. The radiation parameter, α, can be expressed as

$$\alpha = \frac{\tilde{K}_e}{\rho} , \qquad (38)$$

where $\tilde{K}_e$ = Rosseland extinction coefficient and

ρ = packed density of fibrous material.

It is very difficult to accurately model the radiative component of heat transfer. Many other attempts have been made resulting in extremely complicated models; however, the attempt here is only to approximate an order of magnitude to which radiation is attributed.

2.5 *Summary*

For generality, eqn.(37) will be used for the expression of the radiative component. Thus, adding this to the expression derived for the SPCM, the total effective thermal conductivity of a fibrous material taking into account radiation from eqn.(37) can then be expressed as [1]

$$\lambda = \alpha\left(\varepsilon_P\lambda_g + (1 - \varepsilon_P)\lambda_s\right) + (1 - \alpha)\left(\frac{\lambda_s\lambda_g}{\varepsilon_S\lambda_s + (1 - \varepsilon_S)\lambda_g}\right) + 4\sigma\Sigma_T d\, T_m^3 \quad . \qquad (39)$$

The thermal conductivity of the solid phase, λ_s, is a function of temperature, and the thermal conductivity of the gas phase, λ_g, is a function of both temperature and pressure. The effective thermal conductivity of the fibrous material is therefore a function of two variables and four parameters (model constants),

$$\lambda = f(T_m, p; \varepsilon_S, \varepsilon_P, \alpha, \Sigma_T) ,$$

where T_m = mean temperature of the fibrous material,

p = gas pressure,

ε_S = porosity of fibrous material structured in series with heat flow,

ε_P = porosity of fibrous material structured in parallel with heat flow,

α = fraction of fibrous material structured in parallel with heat flow, and

Σ_T = total effective emissivity of the fibrous material.

Similarly, for the UCCM, the effective thermal conductivity of a fibrous material can be expressed as a function of two variables and six parameters,

$$\lambda = f(T_m, p; l_o, l_d, l_{eff}, \phi, h_c A_c, \Sigma_T) .$$

Chapter 3 *Thermal Conduction Due to a Gas*

3.1 *Introduction*

The effect of pressure on the thermal conductivity of a gas can be investigated by using kinetic theory to evaluate the mechanisms which play a role in energy transport within a gas. It can be shown that the energy flux across the y-z plane within a gas is expressed as

$$q_x = -cn\bar{v}\Lambda\frac{d\bar{e}}{dx}, \tag{40}$$

where

n = molecular number density,

$\bar{v}$ = mean velocity of molecule,

Λ = mean free path of molecule,

$\frac{d\bar{e}}{dx}$ = one-dimensional average heat energy gradient in x-dir, and

c = proportionality constant,

which can be found in common texts on gas kinetics. Comparing this equation with the one-dimensional Fourier's law of heat conduction,

$$q_x = -\lambda\frac{dT}{dx}, \tag{41}$$

and recognizing that

$$\frac{d\bar{e}}{dx} = \frac{d\bar{e}}{dT}\frac{dT}{dx}, \tag{42}$$

an expression for the thermal conductivity, λ, is obtained,

$$\lambda = cn\bar{v}\Lambda\frac{d\bar{e}}{dT} . \qquad (43)$$

Now, if the gas is heated at constant volume, the energy input to the gas goes to increasing the internal energy of the gas by increasing the kinetic energy of the molecules. The differential expression for internal energy can be expressed as

$$d\bar{e} = mc_v dT , \qquad (44)$$

where

m = mass of gas,

c_v = specific heat at constant volume, and

dT = differential temperature change.

Recognizing that $m = \rho/n$, eqn.(44) can be stated as

$$n\frac{d\bar{e}}{dT} = \rho c_v . \qquad (45)$$

Substituting eqn.(45) into eqn.(43) yields

$$\lambda = c\rho\bar{v}\Lambda c_v . \qquad (46)$$

The viscosity μ of a gas made up of molecules with translational energy only (i.e., a gas which can be modeled as hard spheres) has been rigorously shown by Kennard [7] to be

$$\mu = \frac{5\pi}{32}\rho\bar{v}\Lambda . \qquad (47)$$

This can be substituted in eqn.(46) to yield

$$\lambda = b\mu c_v , \qquad (48)$$

where

$$b = \frac{32c}{5\pi} . \qquad (49a)$$

From kinetic theory for monatomic molecules, b is exactly 2.5. From experimental data, this is found to be a very good approximation. For polyatomic molecules, b is typically found experimentally to be less than 2.0 [7]. The constant, b, can also be expressed as

$$b = \frac{\gamma}{Pr} \quad , \tag{49b}$$

where γ = specific heat ratio and

Pr = Prandtl number.

It is evident from eqn.(49b) that the constant, b, is independent of pressure; $b \neq f(p)$.

3.2 *Thermal Conduction Derived from Temperature Jump Theory*

Heat conduction of a rarefied gas was first treated by Smoluchowski [8] and later analyzed by Knudsen [9] and others [10, 11]. Knudsen recognized that at low pressures, when a gas can no longer be treated as a continuum, molecules colliding with a boundary surface at some temperature T_w will rebound without perfect transport of energy between the molecule and the boundary; thus, the molecule will have some temperature $T_r \neq T_w$ where T_r is the temperature of the rebounding molecule. Associating an energy E_w with temperature T_w, the imperfect transport of energy can be shown as

$$(E_i - E_r) = a(E_i - E_w) \tag{50}$$

where E_i = energy transferred to boundary surface by incident molecules,

E_r = energy carried away from the boundary after the incident molecule has rebounded,

E_w = energy of rebounded molecules required to be in equilibrium at the boundary temperature, and

a = thermal accommodation coefficient.

Equation (50) states that the mean energy of the molecules re-emitted from the boundary surface is accommodated for by the imperfect energy transport at the boundary. Kennard [7] conjectured an idea of a temperature discontinuity at the boundary and that it could be expressed as

$$T_k - T_w = G\frac{\partial T}{\partial x}\,, \tag{51}$$

where $\frac{\partial T}{\partial x}$ = temperature gradient normal to the boundary surface,

T_k = the boundary temperature that would be obtained if the tangent to the gradient $\frac{\partial T}{\partial x}$ were extrapolated to the boundary, and

G = temperature jump length.

With this, expressions for $(E_i - E_r)$ and $(E_i - E_w)$ can be educed.

Kennard showed that the number of molecules per unit area per unit time crossing a given plane is

$$\Gamma_n = \frac{1}{4}n\bar{v}\,, \tag{52}$$

where

$$\bar{v} = 2\sqrt{\frac{2RT}{\pi}} \tag{53}$$

and is the mean velocity. Multiplying the above expression by the mass of each molecule, m, yields the total mass of molecules per unit area per unit time crossing a given plane and is, for an ideal gas, given by

$$\Gamma_m = \frac{1}{4}\rho\bar{v} = \frac{p}{\sqrt{2\pi RT}}\,, \tag{54}$$

where

p = pressure,

R = gas constant, and

T = temperature.

Kennard concluded that the energy carried by the mass of incident molecules, Γ_m, by a stream issuing from a gas at T_k is

$$E_i' = \Gamma_m(2RT_k + u_k) \ , \tag{55}$$

where $2RT_k$ is the mean translational energy* and u_k is the specific internal energy of the molecules at temperature T_k. Similarly, for a stream issuing from a gas at T_w, the energy transferred can be expressed as

$$E_w = \Gamma_m(2RT_w + u_w). \tag{56}$$

The difference in the two above expressions is

$$E_i' - E_w = \Gamma_m[2R(T_k - T_w) + (u_k - u_w)] \approx \Gamma_m\left[(T_k - T_w)\left(2R + \frac{du}{dT}\right)\right] . \tag{57}$$

According to Kennard, the specific heat at constant volume for molecules possessing translational energy in equilibrium with the wall temperature ($\frac{3}{2}RT$ rather than $2RT$) can be expressed as

$$c_v = \frac{3}{2}R + \frac{du}{dT} \ , \tag{58}$$

thus, the energy of the two streams is

* Kennard showed that the mean translational energy for a gas in equilibrium with the wall is 3/4 of that given above. The increase in energy (2RT rather than 3RT/2) for the nonequilibrium case is attributed to the more numerous high velocity molecules that carry more energy [7].

$$E_i' - E_w = \Gamma_m\left(\frac{1}{2}R + c_v\right)(T_k - T_w) \tag{59}$$

where the $\frac{1}{2}R$ in eqn.(59) is the extra term that appears from the gas/wall nonequilibrium analysis [7]. The total energy due to the incident molecules, E_i, consists of the energy due to E_i' plus the excess energy carried by the stream which contributes to heat conduction. Thus, the sum yields

$$E_i = E_i' + E_c = \Gamma_m(2RT_k + u_k) + \frac{1}{2}\lambda\frac{\partial T}{\partial x} \tag{60}$$

where

E_i' = energy due to incident molecules issuing at T_k,

E_c = excess energy carried by incident molecules due to heat conduction, and

λ = thermal conductivity of gas.

Therefore, the net energy transfer between the two streams can be expressed as

$$E_i - E_w = \frac{1}{2}\lambda\frac{\partial T}{\partial x} + \Gamma_m\left(\frac{1}{2}R + c_v\right)(T_k - T_w)\,. \tag{61}$$

Substituting

$$\frac{1}{2}R + c_v = \frac{1}{2}(\gamma + 1)\,c_v\,, \tag{62}$$

and eqn.(54) into eqn.(61) yields

$$E_i - E_w = \frac{1}{2}\lambda\frac{\partial T}{\partial x} + \frac{1}{2}(\gamma + 1)(T_k - T_w)\frac{c_v p}{\sqrt{2\pi RT}}\,, \tag{63}$$

where γ is the specific heat ratio. The net energy actually transferred by the gas can be simply expressed as the conduction through the gas from a plane normal to the x-coordinate direction; hence,

$$E_i - E_r = \lambda \frac{\partial T}{\partial x} \ . \tag{64}$$

Substituting eqns.(63) and (64) into eqn.(50) yields

$$\lambda \frac{\partial T}{\partial x} = a \left[\frac{1}{2} \lambda \frac{\partial T}{\partial x} + \frac{1}{2} (\gamma + 1)(T_k - T_w) \frac{c_v p}{\sqrt{2\pi RT}} \right] . \tag{65}$$

Rearranging the above expression to be of the form of eqn.(51) and comparing the result yields an expression for G,

$$G = \frac{2 - a}{a} \sqrt{2\pi RT} \frac{\lambda}{(\gamma + 1) c_v p} \ . \tag{66}$$

In order to observe how G is related to the mean free path, Λ, the viscosity is arranged into eqn.(66). Recalling that

$$\mu = \kappa' \rho \bar{v} \Lambda \tag{67}$$

where κ' is a proportionality constant and by replacing ρ with p/RT and $\bar{v}$ with eqn.(53), eqn.(66) becomes

$$G = \frac{2 - a}{a} \frac{4\kappa'}{(\gamma + 1)} \frac{\lambda}{\mu c_v} \Lambda \tag{68a}$$

where $0.491 \leq \kappa' \leq 0.499$ [7]. Substituting eqn.(49b) into eqn.(68a) and setting κ' to 0.5 as for hard elastic sphere model, the temperature jump, G, can be written as

$$G = \frac{2 - a}{a} \frac{2}{(\gamma + 1)} \frac{\gamma}{Pr} \Lambda \ . \tag{68b}$$

For a monatomic gas and a = 1, the coefficient of Λ in eqn.(68b) is

$$\frac{2}{(\gamma + 1)} \frac{\gamma}{Pr} = \frac{15}{8} .$$

Dickins [10] deduced that the heat transfer Q through a rarefied gas between the walls of concentric cylinders can be expressed as

$$Q = \frac{\lambda_g 2\pi l(T_I - T_{II})}{\ln(R_2/R_1) + (G/R_1)} \tag{69}$$

where R_1 and R_2 are the radii of the concentric cylinders and $R_2 > R_1$. The term (G/R_1) is the correction term that Dickins used to accommodate for the temperature jump at the boundary at low pressures. Since the heat transfer, Q, can be expressed as

$$Q = \frac{\lambda_{g\ ref} 2\pi l(T_I - T_{II})}{\ln(R_2/R_1)} \tag{70}$$

where $\lambda_{g\ ref}$ is the thermal conductivity of the gas at ambient pressure, the ratio, therefore, of the thermal conductivity at reduced pressure to that at atmospheric pressure can be expressed as

$$\frac{\lambda_{g\ red}}{\lambda_{g\ ref}} = \frac{\ln(R_2/R_1)}{\ln(R_2/R_1) + (G/R_1)} \ . \tag{71}$$

Now, taking the limiting case for two parallel plates (for $R_1 \approx R_2$), eqn.(71) becomes

$$\lambda_{g\ red} = \frac{\lambda_{g\ ref}\, d}{d + G} \ , \tag{72a}$$

where d is the distance between parallel plates and G is the same as given in eqn(68). Formally, eqn.(69) should have a second temperature jump term associated with the second boundary, R_2; however, G_2/R_2 is thought to be negligible as compared to G_1/R_1 if $R_2 >> R_1$ which was usually the assumption [12]. Therefore, if the second temperature jump is not neglected, eqn.(72a) can be expressed as

$$\lambda_{g\ red} = \frac{\lambda_{g\ ref}\, d}{d + G_1 + G_2} \ . \tag{72b}$$

Lees and Liu [12] used another approach to show that eqn.(71) does not work even when $R_2 >> R_1$. This approach is used herein for the parallel plate case and is discussed in the following section.

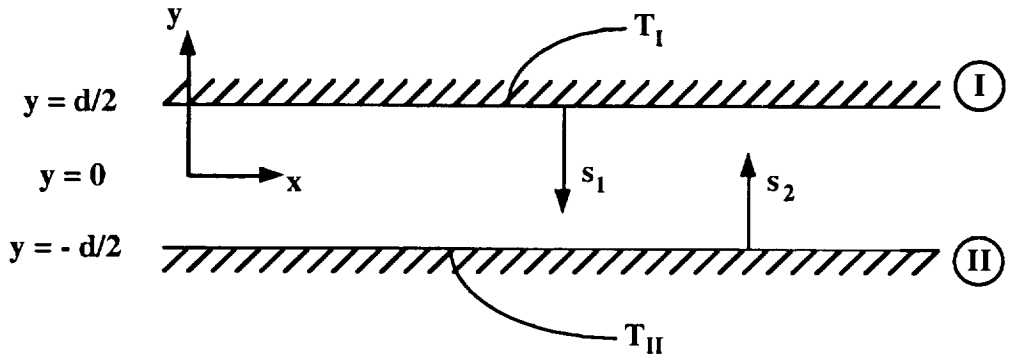

Figure 11. Gas between parallel plates of different temperatures

3.3 *Thermal Conduction Derived from Maxwell Moment Method*

An approach for the thermal conductivity of a gas at reduced pressures is obtained by way of the Maxwell moment method proposed by Lees and Liu [12, 13]. The "two-sided Maxwellian" distribution function which yields the ability to more accurately represent energy transfer in a rarefied gas is incorporated into the derivation. It was experimentally shown that this approach yields better results than expressions obtained by some others [9, 14]. Observing that there are two streams (from the two-sidedness) issuing from two parallel boundary surfaces at temperatures T_I and T_{II} as shown in Fig. 11, it is assumed that each stream, s_1 and s_2, has its own Maxwellian velocity distribution, f_1 and f_2, respectively. The distribution function f is known and is expressed as

$$f = \frac{n}{(2\pi RT)^{3/2}} \exp\left(\frac{-v^2}{2RT}\right). \tag{74}$$

Therefore, for f_1, the expression becomes

$$f_1 = \frac{n_1}{(2\pi RT_1)^{3/2}} \exp\left(\frac{-v^2}{2RT_1}\right), \tag{75}$$

and similarly for f_2. If the mean quantity averaged over all the velocity space is denoted as $\langle\Theta\rangle$, then for any quantity Θ, the mean quantity using the "two-sided Maxwellian" can be expressed as

$$\langle\Theta\rangle = \int \Theta f \, dv = \int_{-\infty}^{\infty}\int_{-\infty}^{0}\int_{-\infty}^{\infty} \Theta f_1 \, dv_x \, dv_y \, dv_z + \int_{-\infty}^{\infty}\int_{0}^{\infty}\int_{-\infty}^{\infty} \Theta f_2 \, dv_x \, dv_y \, dv_z \ . \tag{76}$$

In other words, to find the mean density ρ, let $\Theta = m$; then

$$\rho = \langle m\rangle = \int m f \, dv = \frac{m}{2}(n_1 + n_2). \tag{77}$$

The change in Θ due to molecular collisions, $\Delta\Theta$, in the absence of external forces, is known as Maxwell's integral equation of transfer and in rectangular coordinates is expressed as

$$\Delta\Theta = \frac{\partial}{\partial t}\left(\int \Theta f \, dv\right) + \sum_i \left(\frac{\partial}{\partial x_i}\right)\left(\int \Theta v_i f \, dv\right). \tag{78}$$

The only coordinate direction is y, the direction normal to the parallel surfaces. Therefore, at steady state, eqn.(78) can be reduced to

$$\Delta\Theta = \left(\frac{d}{dy}\right)\left(\int \Theta v_y f \, dv\right). \tag{79}$$

Continuing with the same example as before for mass, the rate of change of mass can now be determined. However, mass is conserved, and therefore $\Delta\Theta = 0$. Then solving for the right side of eqn.(79) and setting it equal to zero yields

$$\frac{k}{\sqrt{2\pi m}}\left(n_2 T_2^{1/2} - n_1 T_1^{1/2}\right) = \Delta\Theta = 0 \tag{80a}$$

or

$$n_2 T_2^{1/2} - n_1 T_1^{1/2} = 0 \,. \tag{80b}$$

In eqn.(80a), k is Boltzmann's constant where $k = mR$.

It is convenient to normalize the variables n_1, n_2, T_1, and T_2. Normalizing with respect to condition I, the following is obtained:

$$\begin{aligned} \bar{n}_1 &= \frac{n_1}{n_I}, \qquad \bar{n}_2 = \frac{n_2}{n_I}, \\ \bar{T}_1 &= \frac{T_1}{T_I}, \qquad \bar{T}_2 = \frac{T_2}{T_I}. \end{aligned} \tag{81}$$

Using the normalized variables, eqn.(80b) becomes

$$\bar{n}_2 \bar{T}_2^{1/2} - \bar{n}_1 \bar{T}_1^{1/2} = 0 \,. \tag{82}$$

To summarize, the expressions for $\langle\Theta\rangle$ and $\Delta\Theta$ are given in Table 1 for continuity, momentum, energy, and heat flux. Note that, according to Fig. 11, the sign of the velocity in the y-coordinate direction determines the Maxwellian distribution used; i.e.,

$$v_y < 0, \qquad f = f_1, \text{ and}$$

$$v_y > 0, \qquad f = f_2 \,.$$

For $\Theta = m$, mv_y, and $\frac{1}{2} mv^2$, the change in Θ due to molecular collisions, $\Delta\Theta$, is zero. However, for $\Theta = \frac{1}{2} mv_y v^2$, the change in Θ can be expressed as

$$\Delta\Theta = -\frac{2}{3}\left(\frac{p}{\mu}\right) q_y$$

and is obtained by evaluating the collision integral (eqn.(79)) using an inverse fifth-power law as the governing force, F, between the particles ($F = \kappa m_1 m_2 / r^5$, where m_1 and m_2 are the masses of the molecules influenced, r is the separation distance, and κ is a constant of proportionality). The expressions for the pressure, viscosity, and the heat flux are given as follows:

$$p = \frac{k}{2}(n_1 T_1 + n_2 T_2)\,, \tag{83}$$

$$\mu = \Lambda \rho \sqrt{\frac{2kT}{\pi m}}\,, \tag{84}$$

and

$$q_y = -\sqrt{\frac{2}{\pi m}}\left[n_1 (kT_1)^{3/2} - n_2 (kT_2)^{3/2}\right]. \tag{85}$$

Table 1. Evaluations of Equations (76) and (79) for given Θ.

Θ	$\langle\Theta\rangle$	$\Delta\Theta$
m	$\frac{m}{2}(n_1 + n_2)$	$\frac{d}{dy}\left\{\frac{1}{\sqrt{2\pi m}}\left[n_2 (kT_2)^{1/2} - n_1 (kT_1)^{1/2}\right]\right\} = 0$
mv_y	$\frac{1}{\sqrt{2\pi m}}\left[n_2 (kT_2)^{1/2} - n_1 (kT_1)^{1/2}\right]$	$\frac{d}{dy}\left\{\frac{k}{2}(n_1 T_1 + n_2 T_2)\right\} = 0$
$\frac{1}{2} mv^2$	$\frac{3}{4}\left[n_1 (kT_1) + n_2 (kT_2)\right]$	$\frac{d}{dy}\left\{-\sqrt{\frac{2}{\pi m}}\left[n_1 (kT_1)^{3/2} - n_2 (kT_2)^{3/2}\right]\right\} = 0$
$\frac{1}{2} mv_y v^2$	$-\sqrt{\frac{2}{\pi m}}\left[n_1 (kT_1)^{3/2} - n_2 (kT_2)^{3/2}\right]$	$\frac{d}{dy}\left\{\frac{5}{4m}\left[n_1 (kT_1)^2 + n_2 (kT_2)^2\right]\right\} = -\frac{2}{3}\left(\frac{p}{\mu}\right) q_y$

Evaluating $\Delta\Theta$ from eqn.(79) for the mass, momentum, energy, and heat flux yields the following normalized equations, respectively:

$$\overline{n}_1\overline{T}_1^{\,1/2} = \overline{n}_2\overline{T}_2^{\,1/2} \qquad \textit{Continuity} \qquad (86a)$$

$$\overline{n}_1\overline{T}_1 + \overline{n}_2\overline{T}_2 = \beta_1 \qquad \textit{Momentum} \qquad (86b)$$

$$\overline{n}_2\overline{T}_2^{\,3/2} - \overline{n}_1\overline{T}_1^{\,3/2} = \beta_2 \qquad \textit{Energy} \qquad (86c)$$

$$\frac{d}{d\overline{y}}\left(\overline{n}_1\overline{T}_1^{\,2} + \overline{n}_2\overline{T}_2^{\,2}\right) + \frac{8}{15}\left(\frac{d}{\Lambda}\right)\beta_2\,\frac{\left(\overline{n}_1\overline{T}_1 + \overline{n}_2\overline{T}_2\right)}{\overline{n}_1 + \overline{n}_2} = 0 \qquad \textit{Heat Flux}^{**} \qquad (86d)$$

These are the four equations and four unknowns to be solved. For a small temperature difference, $T_{II}/T_I \approx 1$, the normalized variables, $\overline{n}_1$, $\overline{n}_2$, $\overline{T}_1$, and $\overline{T}_2$, are very close to unity. Thus, they can be expressed as

$$\begin{aligned} \overline{n}_1 &= 1 + \varepsilon_1\,, & \overline{n}_2 &= 1 + \varepsilon_2\,, \\ \overline{T}_1 &= 1 + \delta_1\,, & \overline{T}_2 &= 1 + \delta_2\,, \end{aligned} \qquad (87)$$

where ε_1, ε_2, δ_1, and $\delta_2 << 1$. Substituting these expressions into eqn.(86) and neglecting terms containing products of any combination of the small perturbation parameters with each other yields

$$\varepsilon_1 + \frac{1}{2}\delta_1 = \varepsilon_2 + \frac{1}{2}\delta_2\,, \qquad (88)$$

$$\varepsilon_1 + \delta_1 + \varepsilon_2 + \delta_2 = \beta_3\,, \qquad (89)$$

$$\varepsilon_2 + \frac{3}{2}\delta_2 - \varepsilon_1 - \frac{3}{2}\delta_1 = \beta_2\,. \qquad (90)$$

From eqns.(88) and (90), it is found that

$$\varepsilon_1 - \varepsilon_2 = \frac{1}{2}\beta_2 \qquad (91)$$

** The present author obtained a slightly different equation for the heat flux than Lees and Liu [12, 13], however, the equation reduces such that the same solution to the system of equations arises as obtained by Lees and Liu.

and

$$\delta_2 - \delta_1 = \beta_2 . \tag{92}$$

Now substituting eqn.(89) into the expression for the heat flux eqn.(86d) yields

$$\frac{d}{d\bar{y}}(\delta_1 + \delta_2) + \frac{8}{15}\left(\frac{d}{\Lambda}\right)\beta_2 = 0 . \tag{93}$$

Integrating eqn.(93) and implementing the boundary conditions,

$$\varepsilon_1 = 0, \delta_1 = 0 \qquad \text{at} \quad \bar{y} = \frac{1}{2} , \tag{94a}$$

$$\delta_2 = -\epsilon \qquad \text{at} \quad \bar{y} = -\frac{1}{2} , \tag{94b}$$

where ϵ is a small perturbation in the temperature ratio,

$$\frac{T_{II}}{T_I} = 1 - \epsilon, \tag{95}$$

the four unknowns can be determined. Solving for the perturbation parameters mentioned in eqn.(87), one obtains

$$\varepsilon_1 = \frac{4}{15}\left(\frac{d}{\Lambda}\right)\beta_2\left(\bar{y} - \frac{1}{2}\right), \tag{96}$$

$$\varepsilon_2 = \beta_2\left[\frac{1}{2} + \frac{4}{15}\left(\frac{d}{\Lambda}\right)\left(\bar{y} - \frac{1}{2}\right)\right], \tag{97}$$

$$\delta_1 = -\frac{4}{15}\left(\frac{d}{\Lambda}\right)\beta_2\left(\bar{y} - \frac{1}{2}\right) , \tag{98}$$

and

$$\delta_2 = -\beta_2\left[1 + \frac{4}{15}\left(\frac{d}{\Lambda}\right)\left(\bar{y} - \frac{1}{2}\right)\right] . \tag{99}$$

Also, the constant β_2 can be expressed as

$$\beta_2 = \frac{\epsilon}{\left[1 + \frac{4}{15}\left(\frac{d}{\Lambda}\right)\right]} . \tag{100}$$

Now denoting the subscript "ref" as the condition of the quantity at ambient conditions and taking the limit of β_2 as the mean free path goes to some small quantity for ambient conditions yields

$$\lim \beta_2 = \lim \frac{\epsilon}{\left[1 + \frac{4}{15}\left(\frac{d}{\Lambda}\right)\right]} = \frac{15}{4}\left(\frac{\Lambda}{d}\right)\epsilon = \beta_{2\,ref} . \qquad (101)$$

Dividing eqn.(100) by (101) yields

$$\frac{q_y}{q_{y\,ref}} = \frac{\lambda_{g\,red}}{\lambda_{g\,ref}} = \frac{\beta_2}{\beta_{2\,ref}} = \frac{1}{1 + \frac{15}{4}\left(\frac{\Lambda}{d}\right)} , \qquad (102)$$

where $\lambda_{g\,red}$ = the thermal conductivity of the rarefied gas and

$\lambda_{g\,ref}$ = the thermal conductivity of the gas at ambient conditions.

Therefore, eqn.(102) can be written as

$$\lambda_{g\,red} = \frac{\lambda_{g\,ref}}{1 + \frac{15}{4}\left(\frac{\Lambda}{d}\right)} , \qquad (103)$$

which is comparable to eqn.(72a) where $\lambda_{g\,ref} = \lambda_g$, but the coefficient of (Λ/d) differs by a factor of 2 when a = 1. Equation (103), however, has been proven to be more accurate for the entire range of pressures [12] and does agree with eqn.(72b) for $G_1 = G_2 = \frac{15}{8}\Lambda$.

3.4 *Mean Free Path*

To evaluate the expression for $\lambda_{g\,red}$, an expression for the mean free path in terms of the pressure and absolute temperature must be obtained. The mean free path of a gas is

the mean distance that a molecule will travel before colliding with another molecule and is expressed as

$$\Lambda = \frac{1}{\sqrt{2}\pi\delta^2 n}, \tag{104}$$

where δ is the molecular diameter. The collision cross-sectional area is the area of influence in which a molecule will collide with another (see Fig. 12). If a molecule approaches a like molecule along a straight path, and the perpendicular distance from the path to the center of the molecule being approached is less than the diameter of the molecule, then the molecules will collide. If this distance is greater than the diameter of the molecule, the molecules will miss. Hence, the collision cross-sectional area is defined as

$$\sigma_c = \pi\delta^2 . \tag{105}$$

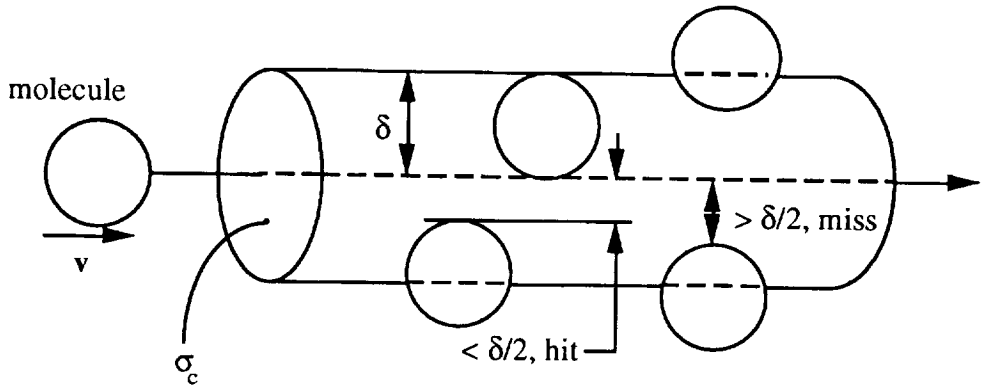

Figure 12. Collision cross-sectional area of influence for a molecule with relative velocity **v**

Substituting the collision cross-section into eqn.(104), the mean free path becomes

$$\Lambda = \frac{1}{\sqrt{2}\sigma_c n} . \tag{106}$$

The number density, n, can be expressed as

$$n = \frac{\rho N_A}{M} , \tag{107}$$

where

N_A = Avagadro's number,

ρ = density of the gas, and

M = molecular weight of the gas.

Replacing the density in eqn.(107) with that obtained from the ideal equation of state yields

$$n = \frac{p}{RT}\frac{N_A}{M} . \tag{108}$$

Substituting this expression into eqn.(104) for the mean free path, Λ, yields

$$\Lambda = \frac{MRT}{\sqrt{2}\sigma_c p N_A} . \tag{109}$$

Recognizing that $MR = \overline{R}$, where $\overline{R}$ is the universal gas constant, eqn.(109) can be expressed as

$$\Lambda = E\frac{T}{p}, \tag{110}$$

where

$$E = \frac{\overline{R}}{\sqrt{2}\sigma_c N_A} . \tag{111}$$

For a gas in a fibrous material, as the pressure is reduced, the mean free path of the gas becomes large with respect to the length scale of the vessel in which the gas is enclosed. The mean free path of a gas in a fibrous material under rarefied conditions can be expressed as

$$\Lambda_o = D\frac{\varepsilon}{1-\varepsilon} , \tag{112}$$

where

Λ_o = mean free path of rarefied gas based on length scale of gas enclosure (mean distance between fibers),

D = mean fiber diameter, and

ε = porosity of the fibrous material.

The mean free path of a rarefied gas between two parallel plates separated by a distance d can be (from definition of *mean beam length*) expressed as

$$\Lambda_o = 2d \, . \tag{113}$$

Yoshida [15] stated that eqn.(113) was invariant to the shapes of the boundary walls enclosing the gas. Therefore, the distance between boundaries, d, could be used to represent the mean distance between fibers. Therefore, from eqns.(112) and (113), eqn.(103) can be expressed as

$$\lambda_{g\,red} = \frac{\lambda_{g\,ref}}{1 + \frac{15}{2}\left(\frac{\Lambda(1-\varepsilon)}{D\varepsilon}\right)} \, . \tag{114a}$$

The thermal conductivity of the gas at reference conditions, $\lambda_{g\,ref}$, is also a function of temperature (see Appendix A) although temperature already appears implicitly in Λ according to eqn.(110).

Equation (114a) can be rewritten as

$$\frac{\lambda_{g\,red}}{\lambda_{g\,ref}} = \frac{1}{1 + \frac{15}{4}\,Kn} \, , \tag{114b}$$

where Kn is the Knudsen number and is expressed as the ratio between the mean free path

of the gas and some characteristic length of the structure enclosing the gas; $Kn = \frac{\Lambda}{d}$. The mean distance between fibers, d, is chosen as the characteristic length. Once Λ becomes significant with respect to d, the gas ceases to behave as a continuum and begins behaving as free molecule flow. Upon rarefaction of the gas (Kn becomes relatively large), $\lambda_{g\,red}/\lambda_{g\,ref}$ approaches zero; as the gas approaches atmospheric conditions (Kn approaches zero), $\lambda_{g\,red}/\lambda_{g\,ref}$ approaches unity (see Appendix B for Kn as a function of pressure). The dynamic region between these extremes is called the *transition* region.

The thermal conductivity of a rarefied gas within a fibrous material is formulated in eqn.(114) and is used for λ_g in eqn.(39). Lees and Liu derived a similar equation in ref[12] for the conductivity of a gas between concentric cylinders that can be expressed as

$$\lambda_{g\,red} = \frac{\lambda_{g\,ref}}{1 + \frac{15}{4}\left(\frac{\Lambda}{R_1}\right)\frac{1}{\ln\left(\frac{R_2}{R_1}\right)}}, \qquad (115)$$

where R_1 and R_2 are the inside and outside radii, respectively. Taking the limit as R_1 approaches R_2 and assigning d as the difference in R_2 and R_1, i.e., $d = R_2 - R_1$, eqn.(115) reduces to eqn.(103) as is expected.

3.5 *Summary*

At low pressures, the mean free path of a gas molecule becomes relatively large with respect to the length scale of the structure enclosing the gas. When this occurs, the gas begins to behave as discrete particles rather than as a continuum. Equation (114) of the previous section expresses the way the thermal conductivity of a gas within a fibrous material varies with pressure. This equation is found by solving for the moments of the

"two-sided" Maxwellian distribution function set forth by Lees and Liu. This yields a system of equations to be solved. This approach is advantageous since the "two-sided Maxwellian" allows for easy implementation of the boundary conditions [12]. The result of the derivation in Section 3.4 (eqn.(114a)) is used in both the SPCM and the UCCM.

Chapter 4 *Experimental Apparatus and Procedure*

4.1 *Introduction*

Experiments were conducted for evaluating the effective thermal conductivity of Nomex® via a double-sided guarded hot plate heater apparatus. This particular apparatus was the Holometrix TCFGM model and conformed to the ASTM C-177 standards [16]. The apparatus operated on the principal of one-dimensional heat transfer. Given an infinite slab of finite thickness with each side held at different but constant temperatures, the thermal conductivity can be determined based on the heat flux through the slab.

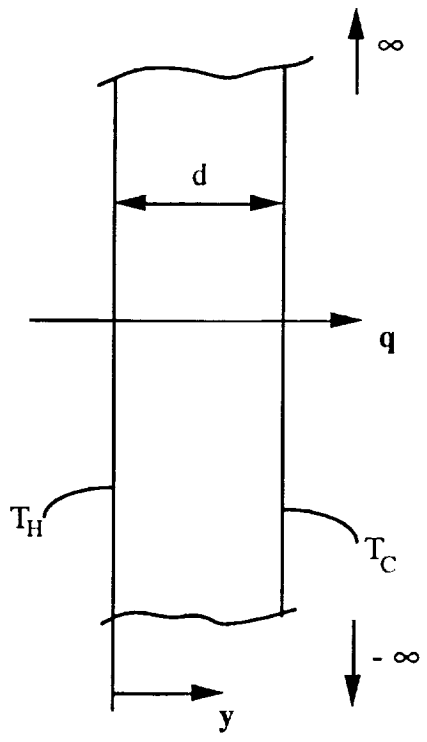

Figure 13. One-dimensional heat transfer through a slab of thickness, d

Obviously, since a real sample has finite surface area, the apparatus must generate as closely as possible one-dimensional heat flow in the metered area that will be observed for the temperature and conductivity measurements; that is, the apparatus must reduce the edge effects so that radial heat transfer is minimized. The center area in which the temperatures are measured and the effective thermal conductivity is calculated is called the metered area. In this metered area, one-dimensional heat flow is acquired and thus simulates the behavior of an infinite slab as shown in Fig. 13.

Data were obtained for various temperatures and fill-gas pressures; i.e., the hot and cold temperatures, T_h and T_c, respectively, were held constant while several test points were obtained over the pressure range from vacuum conditions (~10^{-4} Pa) to atmospheric (101 kPa). The data were collected and used to determine the accuracy of the two mathematical models in their effective thermal conductivity predictions.

4.2 *Test Article Hardware and Description*

The method used in determining the effective thermal conductivity was the guarded hot-plate technique which is illustrated in Fig. 14. The test samples were located between the main/guard heater and the auxiliary heaters. The auxiliary heater was located next to a heat sink and allowed control of the temperature on the cold side of the test sample. The effective thermal conductivity was evaluated from the amount of power supplied to the main heater required to maintain a given temperature difference across the test sample.

An appropriate coolant was supplied to the heat sinks in the test section. Syltherm XLT® (a silicone based heat transfer fluid) was used for ambient testing. For lower

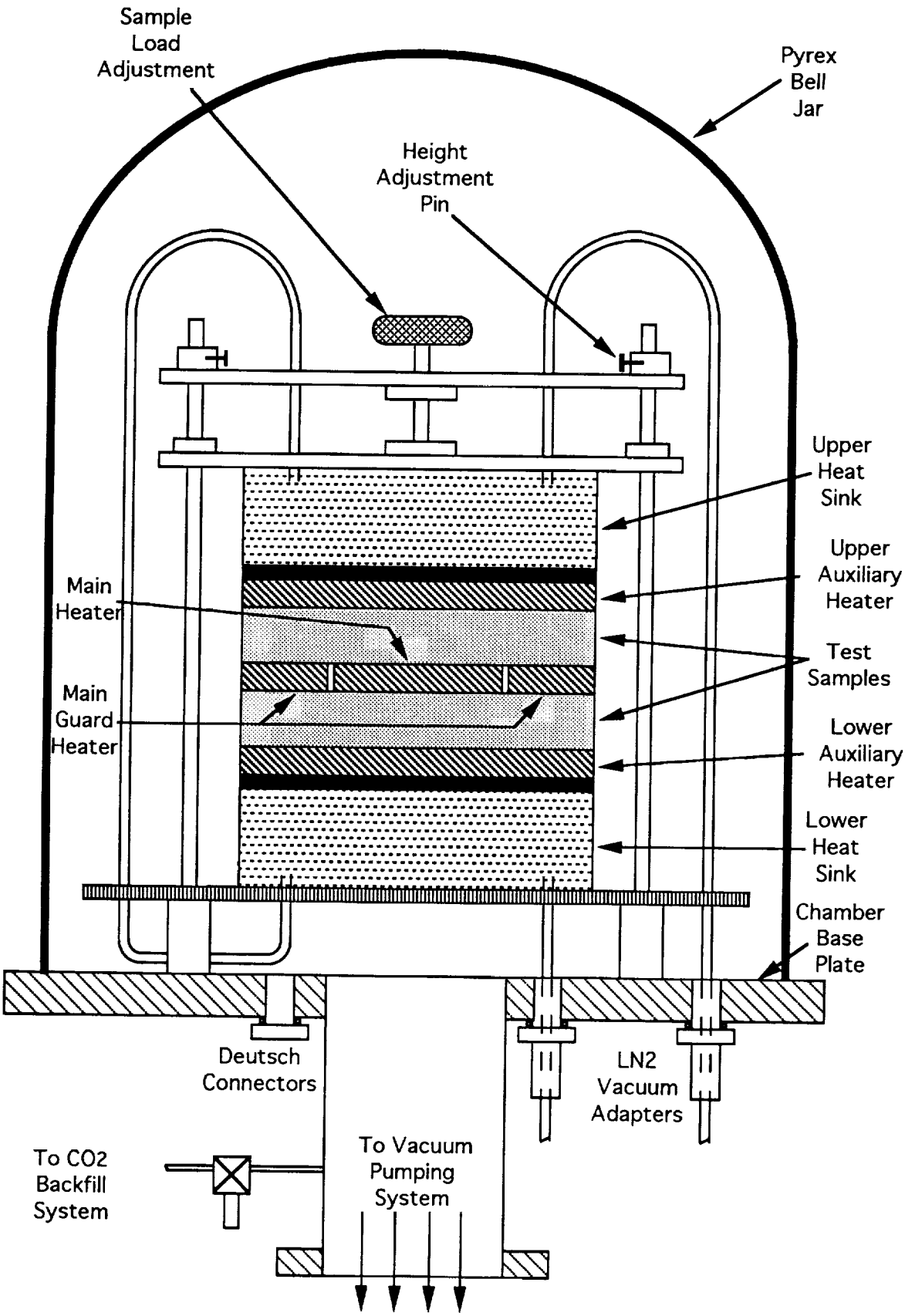

Figure 14. Thermal Conductivity Test Section

temperatures, SylthermXLT or liquid nitrogen was used as the heat sink coolant depending on the set point temperature and fill-gas type.

The temperature difference across the test samples was determined using chromel/alumel (type K) thermocouples. On opposite sides of the test stack were two 6-position terminals for thermocouples (Fig. 15). Sixteen of the total twenty-four thermocouples were used as readout thermocouples while the remaining eight were used as feedback thermocouples. The readout thermocouples were used to measure the temperature of the hot and cold sides of the test samples. The first eight (TC1 - TC8) were mounted in the heater plates while an optional eight (TC9 - TC16) could be mounted on the surface of the test sample. In most cases, the thermal conductance of the sample was low enough to neglect the contact resistance between the heater plate and the test sample surface; therefore, the thermocouples mounted in the heater plates accurately measured the sample surface temperature, and TC9 - TC16 were not necessary. This was a specification set by Holometrix.

The heater set used for the test series consisted of a main/guard heater and two auxiliary heaters. This set had an operating temperature range of -180 °C to 230 °C. The main heater provided the heat flux required to maintain a given temperature difference across the test sample. The thermal power provided by the heater was determined by the electrical power input to the heater; that is, the product of the voltage across the heater and the current through the heater yielded the heat provided to the sample. The guard heater was used to minimize the lateral (or radial) heat transfer at the edges of the main heater. When the control system detected a temperature difference between the main and guard heaters, the power to the guard heater automatically adjusted to eliminate the lateral temperature difference. The auxiliary heaters were controlled to maintain a fixed temperature on the cold side of the test sample. The thermocouples mounted some

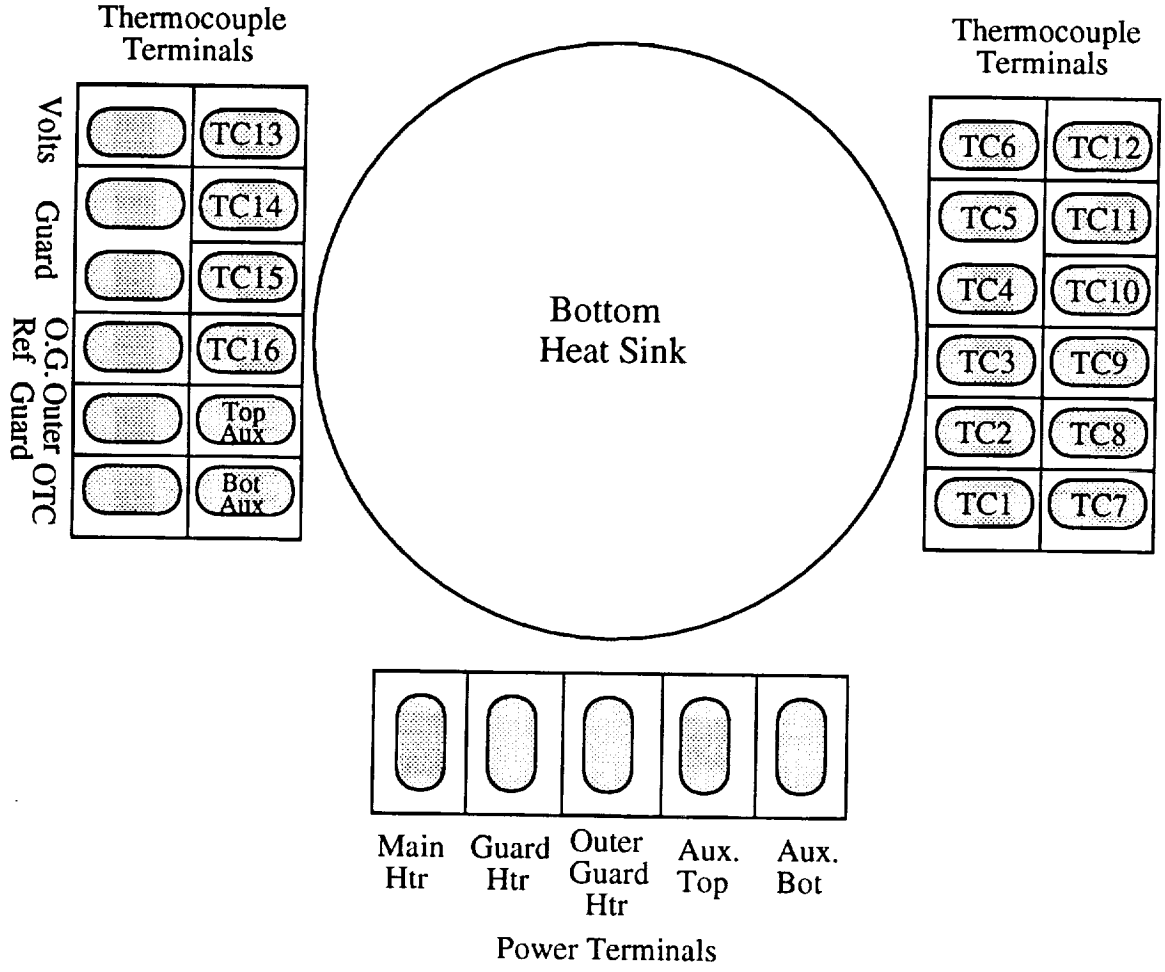

Figure 15. Lay-out of test article base plate terminals

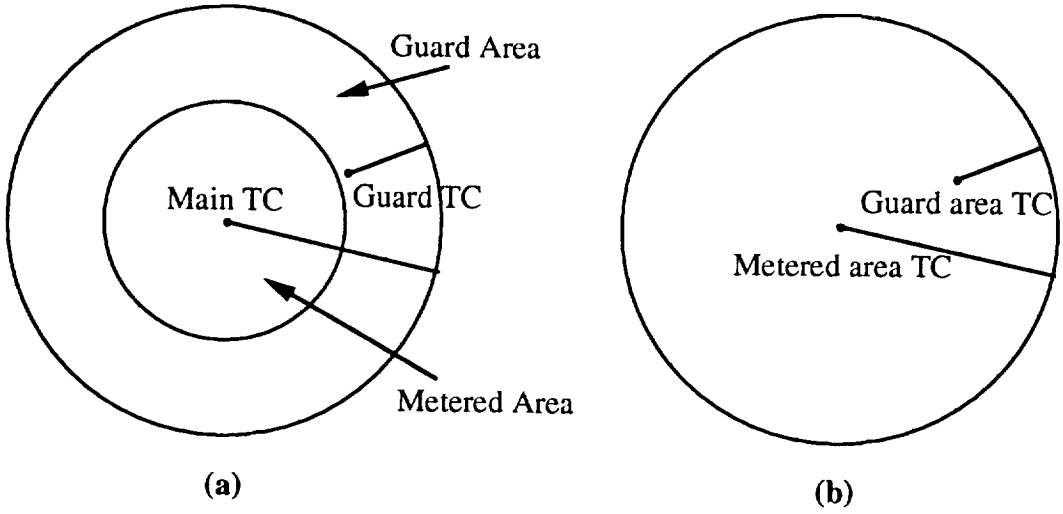

Figure 16. Thermocouple locations: (a) thermocouple location on top face of main/guard heater, (b) thermocouple location on upper auxiliary heater. Same location for bottom face of main/guard and bottom auxilary heaters.

distance away from the center were used to control the power to the guard heater to maintain isothermal conditions in the metered area (for relative thermocouple location, see Fig.16).

The software for the control system monitored the thermocouples on the heater plates. Only the temperature measurements from the thermocouples mounted in the metered area were used to evaluate the effective thermal conductivity of the test sample. The other thermocouples were used for signal feedback to the guard heater controller and for sensor validation. The governing equation used by the software in evaluating the effective thermal conductivity can be expressed as

$$\lambda = \frac{EI}{S}\left[\frac{1}{(\Delta T/d)_1 + (\Delta T/d)_2}\right], \qquad (116)$$

where

E = voltage drop across the main heater,

I = current through the main heater,

S = area of the metered area,

ΔT = temperature difference across the sample, and

d = thickness of the sample,

and the subscripts 1 and 2 denote top and bottom samples.

4.3 *Test Preparation*

The Holometrix TCFGM required two identical samples of the test material eight inches in diameter. The maximum thickness allowed was two inches. Whether it was necessary to mount thermocouples on the sample surface was determined based on the estimated thermal conductance of the material. A low-temperature heater set was chosen

corresponding to the temperature range at which the sample was to be tested (-180 °C to 230 °C). Heater wires and thermocouple leads were checked to insure good condition. The test stack was assembled, and the thermocouple and power leads were connected to the appropriate terminals on the base plate. Once the test stack was assembled, the appropriate coolant fluid was connected to the heat sinks. The test section was subjected to a thermal vacuum environment or some fill-gas at a specified pressure. The computer was programmed with given temperature set points at which the test was to be performed. A Hewlett-Packard Data Acquisition Unit (HP3421A) was used for data acquisition of the main heater power, temperature readout and feedback signals.

4.4 *Test Approach*

The tests were performed in Chamber V (a schematic of Chamber V is shown in Fig. 17) in Building 7, Rm. 2005 at the National Aeronautics and Space Administration - Johnson Space Center. In order to gather data for determining the effect of fill-gas pressure on the thermal performance of insulating materials, the chamber was adjusted to the environmental conditions at which the test article was to be subjected. The chamber was capable of being pumped down to ~10^{-4} Pa (~10^{-6} torr). Either liquid nitrogen or Syltherm XLT® (cryogenic fluid) was used to dissipate the heat of the auxiliary heaters depending on the temperature at which the test was to be performed. A specified fill-gas (air, CO_2, N_2) was allowed to be back-filled into the chamber at prescribed concentrations. The main heater provided the thermal power through the test samples equal to the electrical power input to the main heater. The guard heater was automatically controlled such that the average temperature difference between the main and guard heaters was approximately zero. This minimized the net heat loss in the radial direction. The auxiliary heaters were automatically controlled according to the target temperature selected.

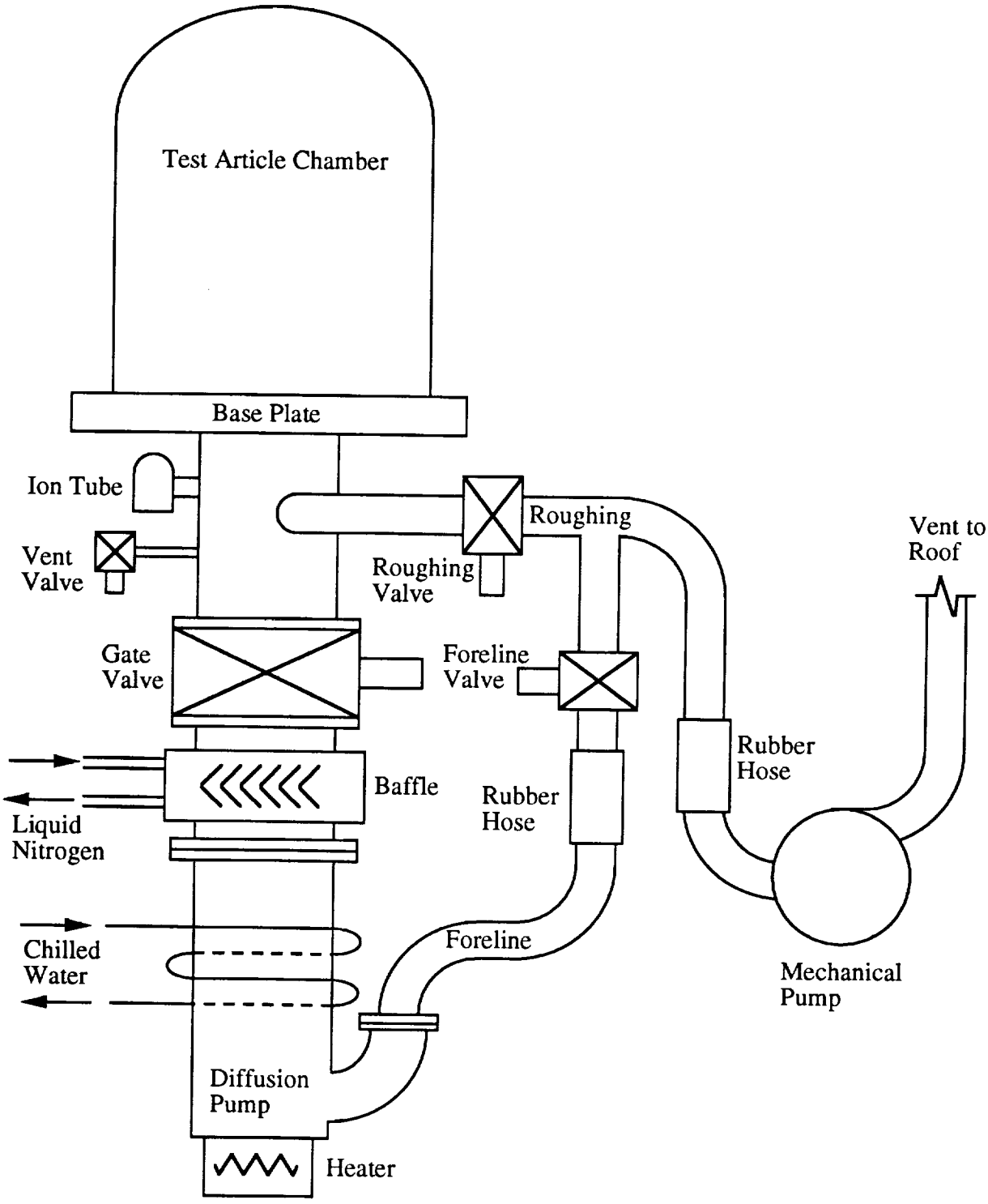

Figure 17. Vacuum Chamber System

The main heater temperatures were sampled every fifteen seconds while all other test article measurements were taken by the computer at a data rate of one sample every sixty seconds. The procedure was repeated for various fill-gas pressures and mean sample temperatures.

4.5 *Data Acquisition*

Data were obtained using the Thermatest Laboratory Automation Software. Three data files containing information about the test instrument, test sample, and range of data to be collected were required for each test run. During the execution of the main program, the computer controlled the power supply and temperature settings and took data readings from the data acquisition unit. Data were periodically printed throughout the duration of the test as temperatures approached equilibrium at time intervals specified by the operator. The computer monitored the temperature readings (every 15 seconds) to determine when changes were small enough to approximate steady state heat flow through the sample and calculated a value for the thermal conductivity of the sample being investigated. The critical temperature data and effective thermal conductivity values were written to an output file. Upon completion of each time interval block of twelve minutes during the test, the temperature, voltage, and current averages were written to a second output file. Hence, a total of five files were associated with each test run.

4.6 *Test Duration*

A typical test took from 4 to 10 hours to reach steady state conditions in the test section. The time required for thermal equilibrium was a function of the mass and thermal diffusivity of the test sample and the operating temperatures.

Chapter 5 *Method of Correlation of Experimental Data with Model*

5.1 *Correlation of the SPCM*

The structural parameters α, ε_S, and ε_P of the Series/Parallel Conduction Model are determined from experimental test points for air at 20°C by using a best-fit technique. Initially assuming that $\lambda_{vac} = \lambda_R$ and subtracting λ_R from λ_{exp}, eqn.(4) is used as a first approximation of the structural parameters. Only two of the three parameters are unknown since the third can always be solved using eqn.(5). After the structural parameters are determined, the thermal conductivity due to pure solid conduction is evaluated from

$$\lambda_F = \alpha(1 - \varepsilon_P)\lambda_s \qquad (117)$$

and compared with the experimental value, λ_{vac}, obtained at high vacuum (~ 10^{-5} mmHg). The experiment that is conducted at high vacuum yields the effective thermal conductivity due to pure solid conduction and radiation, $\lambda_F + \lambda_R = \lambda_{vac}$. Thus, a value for the radiative conductivity, λ_R, is determined (the effective thermal conductivity at vacuum conditions was measured at 0.0034 W/m°C for Nomex at 93% porosity and thickness of 12mm). By rearranging eqn.(1), λ_R is subtracted from the experimental data to yield values without the effects of radiation; hence

$$\lambda_{exp} - \lambda_R = \lambda_F + \lambda_G.$$

The parameters are solved once again but for $\lambda_{exp} - \lambda_R$ rather than λ_{exp}. Then a best-fit curve is adjusted to the modified data to obtain new values for the parameters. The new

parameters are again used to evaluate λ_F and compared to λ_{vac}. This is repeated until the values of the structural parameters converge. This procedure is illustrated in Fig. 18.

5.2 *Correlation of the UCCM*

The parameters for the Unit Cell Conduction Model include ϕ, l_{eff}, and h_cA_c. The effective thermal conductivity measured under vacuum conditions is assumed to be attributed solely to radiation (in other words, neglecting solid conduction through fibers and fiber contact points). This yields a rough estimate of the effective emissivity Σ_T from eqn.(35). The parameters ϕ and l_{eff} are evaluated from experimental data assuming h_cA_c is negligible at pressures close to atmospheric. From the values of ϕ and l_{eff}, h_cA_c is determined from the experimental points in the entire range of pressures. The difference in the calculated value at a vacuum and the experimental value is assigned as the contribution due to radiation. A new value for the effective emissivity Σ_T is calculated, and the procedure is repeated. This procedure is illustrated in Fig. 19.

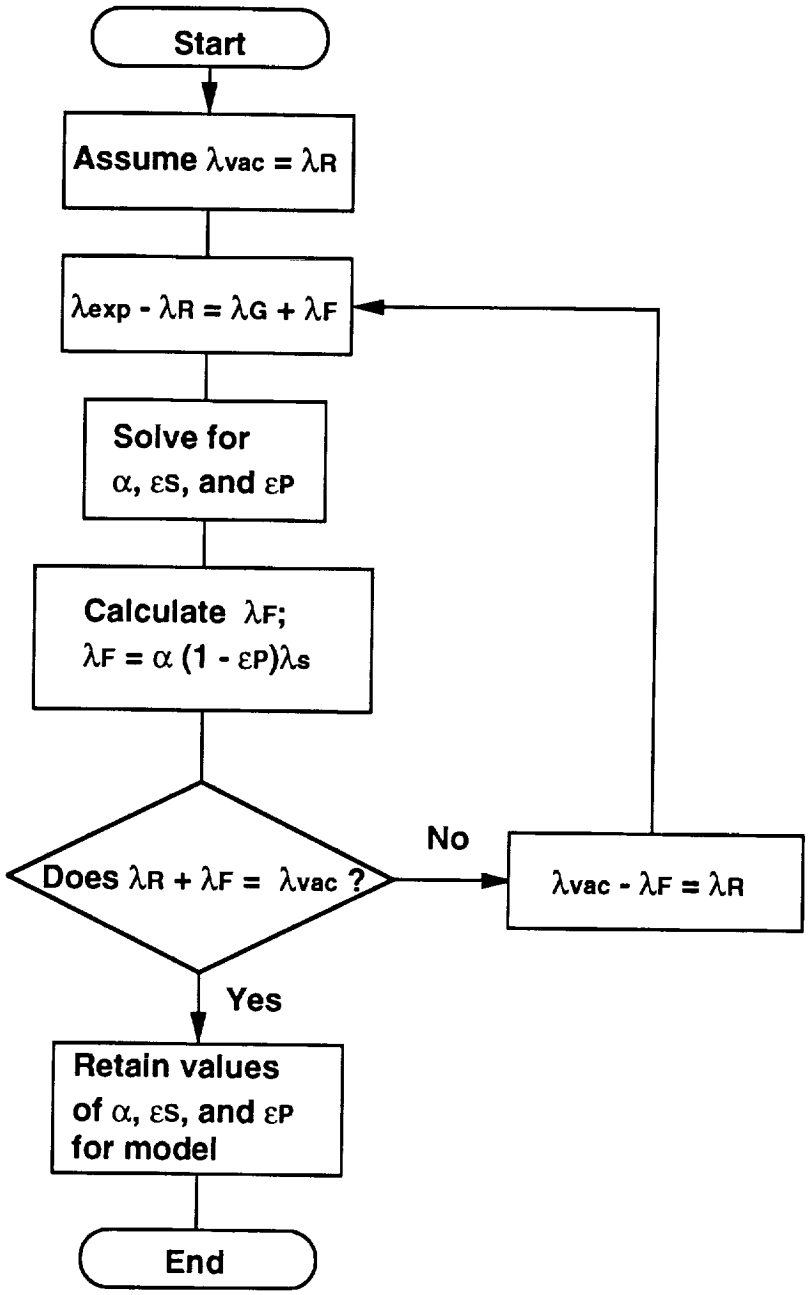

Figure 18. Flowchart of iterations for SPCM

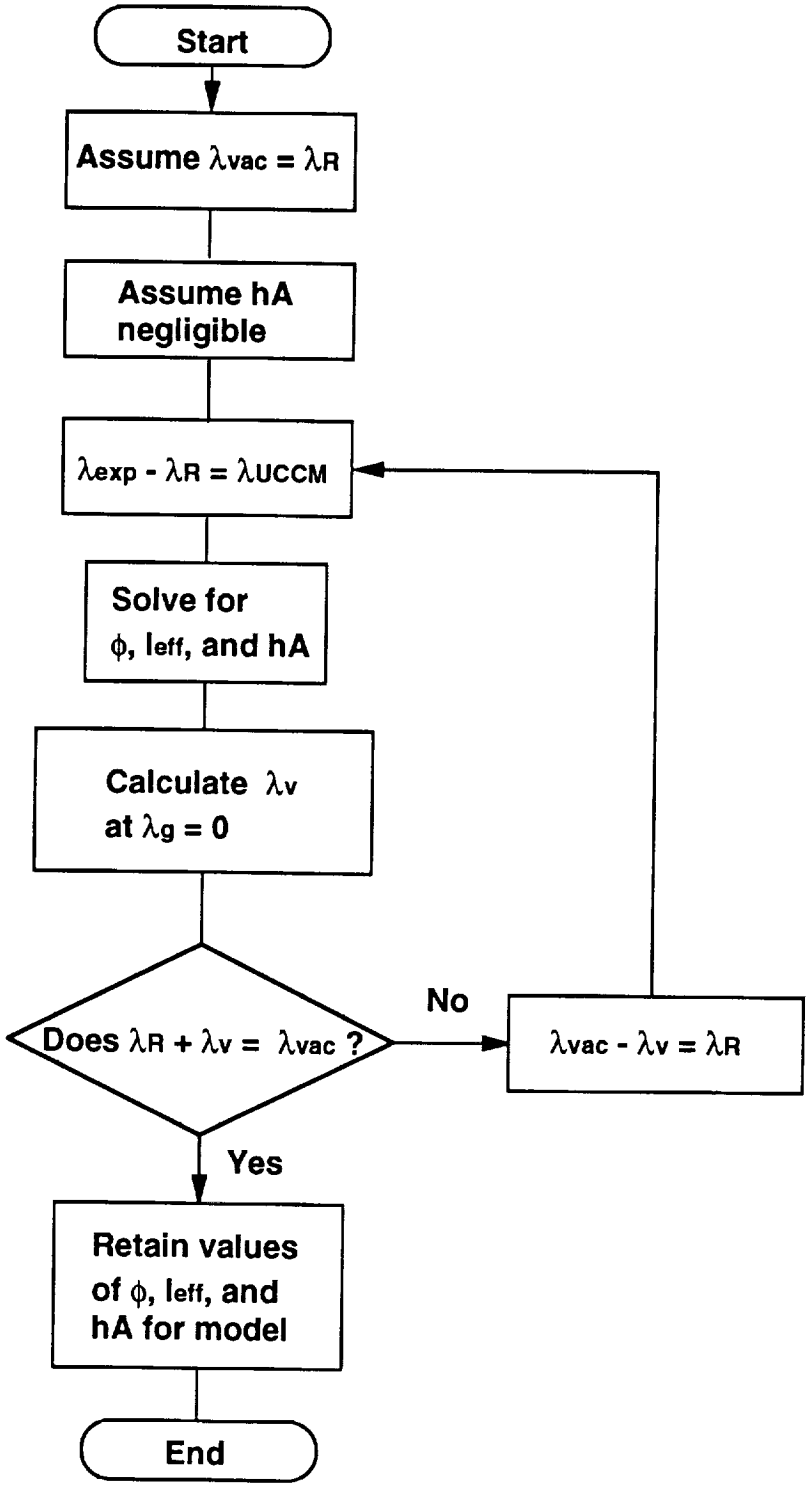

Figure 19. Flowchart of iterations for UCCM

Chapter 6 *Uncertainty Analysis*

6.1 *Introduction*

Most experiments require several primary measurements to calculate the result being sought. It is of interest to determine the uncertainty of the final result given the uncertainty of each of the primary measurements, or *measurands*. There are a number of ways to do this, but the method of weighted residuals was employed here.

The method of weighted residuals implements the idea that uncertainties carried by various parameters being measured are weighted according to the "amount" of influence that they have on the uncertainty of the final result. This influence is called *sensitivity*. If w_g is the uncertainty in some function $g(x_1, x_2, ..., x_n)$, where g is the result, and w_1, w_2, ..., w_n are the uncertainties in the primary measurements $x_1, x_2, ..., x_n$, respectively, then the uncertainty in g may be calculated as

$$w_g = \left[\left(\frac{\partial g}{\partial x_1} w_1\right)^2 + \left(\frac{\partial g}{\partial x_2} w_2\right)^2 + \cdots + \left(\frac{\partial g}{\partial x_n} w_n\right)^2\right]^{1/2}, \qquad (118)$$

where $\frac{\partial g}{\partial x_i}$ are the appropriate weighting terms corresponding to the uncertainty w_i. The function used to calculate the effective thermal conductivity of the fibrous material is given in eqn.(116). Letting $\lambda = g$, eqn.(118) becomes

$$w_\lambda = \left[\left(\frac{\partial \lambda}{\partial x_1} w_1\right)^2 + \left(\frac{\partial \lambda}{\partial x_2} w_2\right)^2 + \cdots + \left(\frac{\partial \lambda}{\partial x_n} w_n\right)^2\right]^{1/2}, \qquad (119)$$

where the measurands required to solve eqn.(116) are $(\Delta T)_1$, $(\Delta T)_2$, d_1, d_2, E, I, and S. Therefore, the following sensitivities are as follows:

$$\frac{\partial \lambda}{\partial (\Delta T)_1} = - \frac{EI}{Sd_1} \left[\left(\frac{\Delta T}{d} \right)_1 + \left(\frac{\Delta T}{d} \right)_2 \right]^{-2},$$

$$\frac{\partial \lambda}{\partial (\Delta T)_2} = - \frac{EI}{Sd_2} \left[\left(\frac{\Delta T}{d} \right)_1 + \left(\frac{\Delta T}{d} \right)_2 \right]^{-2},$$

$$\frac{\partial \lambda}{\partial d_1} = \frac{EI}{S} \left(\frac{\Delta T}{d^2} \right)_1 \left[\left(\frac{\Delta T}{d} \right)_1 + \left(\frac{\Delta T}{d} \right)_2 \right]^{-2},$$

$$\frac{\partial \lambda}{\partial d_2} = \frac{EI}{S} \left(\frac{\Delta T}{d^2} \right)_2 \left[\left(\frac{\Delta T}{d} \right)_1 + \left(\frac{\Delta T}{d} \right)_2 \right]^{-2}, \qquad (120)$$

$$\frac{\partial \lambda}{\partial E} = \frac{I}{S} \left[\left(\frac{\Delta T}{d} \right)_1 + \left(\frac{\Delta T}{d} \right)_2 \right]^{-1},$$

$$\frac{\partial \lambda}{\partial I} = \frac{E}{S} \left[\left(\frac{\Delta T}{d} \right)_1 + \left(\frac{\Delta T}{d} \right)_2 \right]^{-1},$$

and

$$\frac{\partial \lambda}{\partial S} = - \frac{EI}{S^2} \left[\left(\frac{\Delta T}{d} \right)_1 + \left(\frac{\Delta T}{d} \right)_2 \right]^{-1}.$$

If the governing equation of a particular measurement is complicated such that the partial derivatives (sensitivities) are not easily obtainable, another way of determining the uncertainty in a calculation can be expressed as

$$\frac{w_\lambda}{\lambda} = \left[\left(a_1 \frac{w_1}{x_1} \right)^2 + \left(a_2 \frac{w_2}{x_2} \right)^2 + \cdots + \left(a_n \frac{w_n}{x_n} \right)^2 \right]^{1/2}, \qquad (121a)$$

where a_i is the power, or order, to which λ depends on the measurand x_i. Although the exact equation used in calculating the effective thermal conductivity is known, eqn.(121a) is desirable since other uncertainties not appearing explicitly in eqn.(116) could be accounted. By using eqn.(121a) and assuming for now that the a_i's are equal to unity, the uncertainty in the measured value of effective thermal conductivity using a guarded hot-plate heater apparatus can be expressed as

$$\frac{w_\lambda}{\lambda} = \left[\left(\frac{w_{\Delta T}}{\Delta T}\right)^2 + \left(\frac{w_d}{d}\right)^2 + \left(\frac{w_{Q_g}}{Q_g}\right)^2 + \left(\frac{w_{Q_{edge}}}{Q_{edge}}\right)^2 + \left(\frac{w_Q}{Q}\right)^2\right]^{1/2}, \qquad (121b)$$

where

ΔT = temperature difference across sample,

d = sample thickness,

Q_g = gap heat flow,

Q_{edge} = gap heat flow, and

Q = heater power.

The uncertainties in Q_g and Q_{edge}, w_{Q_g} *and* $w_{Q_{edge}}$, are system errors and could be neglected if only first order uncertainties are to be considered. The magnitudes of Q_g and Q_{edge} are determined to be negligible when compared to Q; therefore, even if w_{Q_g} and $w_{Q_{edge}}$ are relatively large with respect to the largest stochastic uncertainty, the effect on the overall first order uncertainty is negligible. The uncertainties in the heater power and the temperature difference will themselves have to be determined by eqns.(118) or (121a) since they are governed by equations that have uncertainties within their independent variables.

The internal calculation of the effective thermal conductivity that the guarded-hot plate apparatus measures is independent of the pressure. The pressure within the chamber is recorded at the time the test point is obtained and is not actually used in calculating the effective thermal conductivity. However, since the premise of the research is to observe the effects of pressure as an independent variable on the thermal conductivity measurements, the uncertainty of the pressure measurements are taken into account separately. For this reason, pressure does not appear in eqn.(121b).

6.2 *Individual Uncertainties*

The measurements taken into consideration that contribute to the overall uncertainty are: plate temperatures and mean temperature, meter area heat flow, gap heat flow, net heat flow at sample edge, fill-gas pressure, and sample thickness. Each of these measurements are analyzed for their individual contribution to the overall uncertainty.

6.2.1 *Meter Area Heat Flow*

The meter area heat flow is given by the product of the voltage across the main heater and the current through the main heater. A regulated DC power supply provides power to the main heater with a maximum output of 40 V and power of 200 W. A HP3421A data acquisition unit is used that has a digital multimeter with 5.5, 4.5, and 3.5 digit resolutions. Frequency counter and thermocouple compensation are built into the data acquisition unit. All specifications provided by Hewlett Packard for the HP3421A are for relative humidity $\leq 85\%$ at 30 °C.

Uncertainties vary depending on the magnitude of the actual reading and the scale of the instrument in which it is read. As an example, a measurement of a 1.4V signal taken on a 3V range with 5.5 digit accuracy is given by

$$\pm (\%\ \text{reading} + \text{counts}) = \pm (0.00009(1.4\text{V}) + 0.00003)$$

$$= \pm 0.156\ \text{mV}.$$

As a percentage, the uncertainty in heater voltage is

$$\frac{0.156(10)^{-3}}{1.4\text{V}}(100) = 0.011\%$$

Therefore, the percentage uncertainty is ± 0.011%. For a 0.5 V signal measured on the same range and with the same resolution, the percentage uncertainty becomes 0.015%. A main heater power of ~0.3W is associated with a heater voltage, V_h, of 1.4 V. Since the heater resistance, R_h, is ~7.09 Ω, and the shunt resistance, R_s, is 0.01 Ω, then $V_h \approx 710V_s$. Also, since the main heater power can be determined by

$$Q_m = \frac{V_h V_s}{R_s}, \tag{122}$$

then the shunt voltage can be expressed as

$$V_s = \sqrt{\frac{Q_m R_s}{710\Omega}}. \tag{123}$$

According to eqn.(123), $V_s \approx 2$ mV. Therefore, the approximate uncertainty on a 0.3 V scale with six counts and a minimum detectable signal of 1 μV is 0.31%. This obviously dominates over the uncertainty in the heater voltage. The uncertainty in R_s is assumed negligible. Therefore, the uncertainty in the heater power is taken as that of the uncertainty in V_s.

6.2.2 *Plate Temperature, Temperature Difference, and Mean Sample Temperature*

The hot and cold plate temperatures are measured using chromel/alumel (Type K) thermocouples. The uncertainty of the thermocouples is given by the manufacturers as ±2.2 °C (or ±0.75%) ≥ 0 °C and ±2% < 0 °C. However, an uncertainty of only ±0.5 °C is used in calculating $w_{\Delta T}$ since the thermocouples are validated against one another and found to have a precision of ±0.1 °C. In this case, precision may be more important than accuracy when considering temperature difference.

From the above information, the uncertainty in the temperature difference $w_{\Delta T}$ can

be determined. Since $\Delta T = T_H - T_C$, the uncertainty in the temperature difference can be expressed as

$$w_{\Delta T} = \left[\left(w_{T_H} \frac{\partial(\Delta T)}{\partial T_H} \right)^2 + \left(w_{T_C} \frac{\partial(\Delta T)}{\partial T_C} \right)^2 \right]^{1/2} \qquad (124)$$

where

$$\frac{\partial(\Delta T)}{\partial T_H} = 1,$$

$$\frac{\partial(\Delta T)}{\partial T_C} = -1,$$

$$w_{T_H} = \pm 0.5 \text{ °C, and}$$

$$w_{T_C} = \pm 0.5 \text{ °C.}$$

With this, eqn.(124) yields an uncertainty of ± 0.7 °C. Similarly for the mean sample temperature which can be expressed as

$$T_m = \frac{T_H + T_C}{2}, \qquad (125)$$

the uncertainty w_{T_m} is ± 0.35 °C.

6.2.3 *Sample Thickness*

Low density, compressible samples require spacers to support the weight of the heaters in the test stack to prevent compression of the samples beyond the desired thickness. The sample thickness, d, is determined by measuring the thickness of the spacers using calipers. The uncertainty in the measurements using the calipers has not been calculated but has been approximated as ±25 μm. Based on order of magnitude, this seems a reasonable estimate. This uncertainty (±25 μm) was used for a similar measurement by the National Bureau of Standards (NBS) [17].

6.2.4 *Gap Heat Flow*

The simplest way for evaluating the error due to the gap heat flow is to measure it empirically [17]. However, data have not been obtained to determine how the meter-area heat flux, Q_m, has been affected by the gap voltage, V_g. Thus, a gap theory for the main and guard heaters developed by the NBS is employed to determine the error.

The gap heat flow Q_g was shown by Woodside [18] to be

$$Q_g = (q_o + c\lambda)\Delta T_g \, . \tag{126}$$

This equation is the heat flow between the main heater and the guard heater as a result of a temperature difference between the outer edge of the main heater and the inner edge of the guard heater. The term q_o is the heat flow per unit temperature that transfers immediately across the gap while $c\lambda$ is the term for the portion of heat per unit temperature that flows radially through the sample across the gap region. The gap heat flow can also be expressed as

$$Q_g = S_g S_{tc} \Delta T_g \, , \tag{127}$$

where

S_g = heat flow sensitivity per unit voltage,

S_{tc} = thermocouple sensitivity, and

ΔT_g = gap temperature difference.

Therefore, the product of the sensitivities can be expressed as

$$\frac{Q_g}{\Delta T_g} = S_g S_{tc} = q_o + c\lambda \, . \tag{128}$$

The parameter c is a function of the dimensions of the apparatus and can be expressed as [17, 18]

$$c \approx \frac{P}{72\pi} \ln(4a) , \tag{129}$$

where

$$a = \frac{e^z}{e^z - 1} ,$$

d_g = one half the gap width,

P = gap perimeter measured from meter area radius,

d = specimen thickness, and

$$z = \frac{2\pi d_g}{d} .$$

The following values are determined for the Holometrix Model TCFGM: $c \approx 0.00354$, $a = 3.0791$, $d_g = 0.75$ mm, P = 0.3192m, d = 0.012 m, and $z = 0.3927$. For chromel/alumel thermocouples, the thermocouple sensitivity is evaluated as

$$S_{tc} \approx (20\ \mu V/°C/\text{stage})(5\ \text{stages}) = 200\ \mu V/°C.$$

The heat flow sensitivity, S_g, is approximately 2 mW/μV. This is a conservative estimate of the heat flow sensitivity based on only a few measurements of the gap voltage and the corresponding main heater power. The heat flow per unit temperature that flows immediately across the gap is estimated as

$$\begin{aligned} q_o &= (0.002\ W/\mu V)(200\ \mu V/°C) \\ &= 0.4\ W/°C. \end{aligned}$$

The remaining portion of heat flow per unit temperature across the gap for $\lambda =$ 0.0325W/m°C is

$$c\lambda = 1.15(10)^{-4}\ W/°C.$$

It is noted that $q_o >> c\lambda$; that is, most of the heat flow across the gap region occurs at the plate surface rather than in the fibrous material. This, also, was shown to be the case for the NBS analysis [17].

6.2.5 *Net Heat Flow at Sample Edge*

To minimize the edge effects, two data sets are taken at a mean temperature of 20°C with a ΔT of 20°C. The ambient temperature is approximately 24°C. One would expect that in order to reduce the edge effects, the ambient temperature should equal the mean sample temperature. This would be true if the heat flow which is calculated from the power to the main heater were actually determined at the plane intersecting at half the distance between the hot and cold plates. But since the heat flow is determined at the meter area hot-plate, the ambient temperature needs to be greater than the mean sample temperature to reduce the edge effects [17, 19]. This is the premise for choosing 20°C as the set point temperature.

The NBS conducted tests on a larger guarded hot plate (1016 mm diameter) in which the sample thickness to heater plate diameter ratio was 0.07 and 0.15. For both of these, it has been determined that the edge effects were negligible. Since the sample thickness to heater plate diameter ratio is approximately 0.06 for the TCFGM, the edge effect is assumed to be negligible, also.

6.2.6 *Fill-Gas Pressure*

The fill-gas pressure is measured by a 19 psia Ruska Gage for pressures greater

than 1 mmHg while a 1 torr barotron is used for pressures less than 1 mmHg. The accuracy of the Ruska Gage for warm-up times greater than 90 minutes is 0.01% full scale. This includes the uncertainty of linearity, repeatability, hysteresis, and temperature compensation. The 1 torr barotron is accurate to within 0.15% of reading ± temperature coefficients.

Chapter 7 *Results of Model and Data Comparison*

7.1 *Overview*

Two models for predicting the effective thermal conductivity of a fibrous material are proposed. Both models account for the thermal conductivity due to solid conduction, gaseous conduction, and conduction due to the influence of radiation. A double-sided guarded-hot plate heater apparatus is used to determine the effective thermal conductivity of Nomex for various atmospheres. Tests are conducted with air at 20°C, CO_2 at 20°C, 0°C, and -30°C, and N_2 at -50°C for a range of pressures varying from vacuum (~10^{-4} Pa) to atmospheric conditions (10^5 Pa). The Series/Parallel Conduction Model (SPCM) correlates very well to the experimental data; however, a correction factor has to be introduced for the gas conductivity when analyzing CO_2. This is thought to be due to CO_2 being a polyatomic molecule as opposed to a monatomic or diatomic molecule. The Unit Cell Conduction Model (UCCM) also correlates well to the experimental data. The same correction factor for CO_2 conductivity, as in the SPCM, is used since the gas conductivity within a fibrous material is a function of the mean distance between fibers and not the particular model used.

7.2 *Reference Data*

Comparison of the models with the experimental data is done by calibrating to the model one set of data to obtain certain parameters that are specific to the fibrous material and are independent of the set point (independent of temperature and pressure). With

these parameters held constant, the model is used to compare with the other data sets at different temperatures.

The data for air at a mean sample temperature of 20°C is used as the reference data. The other data sets are used to determine the accuracy of the model predictions. The physical parameters of both models are calculated to "best fit" the reference data. The data set for air at 20°C is chosen as the reference set since air consists primarily of diatomic molecules for which the gas conduction equation is valid (more valid than for polyatomic molecules). The data set was obtained at 20 °C and is chosen for the reasons concerning the minimization of edge effects discussed in Section 6.2.5. This set is also desirable since λ_s is most accurately known at approximately 20°C. The test series for air and CO_2 at 20°C were conducted a second time to verify the repeatability of the test points.

7.3 *Physical Parameters*

Several physical parameters of Nomex are necessary to evaluate the performance of the models. Du Pont®, who manufactured the Nomex filament yarn, supplied some of the requisite information. The bulk solid thermal conductivity (thermal conductivity of the material of which the fibers were made), λ_s, is given as 0.13 W/m°C at 22°C [20]. Nothing is known of how λ_s varies with temperature; therefore, it is assumed to be relatively constant for the temperature range for which the tests are conducted. The fiber diameter is given as 0.015 - 0.017mm[§]. The density of the bulk solid is approximately 1443 kg/m^3. The fibrous material is tested at a density of 101 kg/m^3. This corresponds to a porosity of ~0.93. For the UCCM, the *maximum* density, ρ_o, of the fibrous material

[§] The cross-section of a Nomex fiber is typically oval or dog-bone in shape. The values given by Du Pont were for the widest section of the fiber [20]. For this research, the fiber diameter was taken to be ~0.014 mm to compensate for the noncircular cross-section.

is needed. The maximum density is the density at which the fracture of fibers is imminent. This is determined to be ~1213 kg/m^3 (see Appendix C).

7.4 *SPCM Correlation*

The SPCM parameters are examined for the reasonableness of their magnitudes. The structural parameter α, which designates the fraction of the fibrous material that could be considered structured in parallel to the direction of heat flow, is determined to be 0.949; that is, 94.9% when correlated to the reference data. This seems rather high when one considers that the majority of the fibers physically lie in planes normal to the direction of heat flow. Therefore, one might conclude that a larger fraction of the material should be considered to be in series with respect to the direction of heat flow. But if one considers the voids and solid phase regions rather than the solid fibers themselves, it becomes evident that the void channels are for the most part continuous for open-pore systems. Thus, it seems reasonable to conclude that if the majority of void channels could be considered oriented parallel to the direction of heat flow, then so must also the solid phase regions. Bankvall [1] and Strong [2] also obtained values of $\alpha \geq 0.9$ using similar models.

Because of the large value of α, the value for the porosity of the portion of the fibrous material considered to be in series with respect to heat flow, ε_S, is expected to be small. This is found to be true and is determined to be 0.015. The remaining structural parameter, ε_P, the porosity of the portion of the fibrous material in parallel with respect to heat flow, is solved from eqn.(5) and found to be 0.979. Finally, the effective emissivity, Σ_T, is found to be approximately 0.012 corresponding to the contribution to radiation of $8.24(10^{-4})$ W/m°C. These parameters are determined from the set of data obtained for air

at a mean sample temperature of 20°C. Once these parameters are found, they are held fixed since they are considered to be characteristic of the physical structure of the material. The model is then evaluated for the remaining sets of data to determine the degree of accuracy with which the model could predict for various other conditions the effective thermal conductivity of Nomex.

The SPCM correlates very well to all the data sets as demonstrated in Figures 22, 24, and 26. However, in order to accurately predict the effective thermal conductivity in a CO_2 environment, a correction factor had to be applied to eqn.(114a) for the gas thermal conductivity. Thus, eqn.(114a) is modified and expressed as

$$\lambda_{g\ red} = K \frac{\lambda_{g\ ref}}{1 + \frac{15}{2}\left(\frac{\Lambda(1 - \varepsilon)}{D\varepsilon}\right)}, \qquad (130)$$

where K is a correction factor for the thermal conductivity of CO_2 and is determined to be about 0.9. It is assumed that the complexity of CO_2 molecules as opposed to monatomic or diatomic molecules is the reason for the necessity for K. Initially, K was thought to be dependent upon the intermolecular forces between the molecules of the gas. However, even though an inverse fifth power law is used as the governing repulsive force in deriving the gas conduction equation, higher inverse powers were tried and not found to affect the thermal conductivity significantly. In fact, intermolecular force, collision cross-section, and viscosity do not even alter the limits of eqn.(114) since the ratio $\lambda_{g\ red}/\lambda_{g\ ref}$ is always bounded by the interval [0, 1) and never [0, x] where $x < 1$; e.g., $x = 0.9$. Therefore, K must in some way be a function of the physical structure of the material. This leads to the following conjecture.

Since the effective pore size of an open pore system is not physically well defined

due to fiber bundles and protruding free ends of fibers, one might conclude as did Williams and Curry [21] that the thermal conductivity of a gas within a fibrous material would require a correction factor. Williams and Curry proposed a correction factor that was independent of the gas type and was based purely on temperature, pressure, and an additional empirical factor which was density dependent. However, the approach taken herein for obtaining an expression for the thermal conductivity of a gas is different than that proposed by Williams and Curry, so the correction factor is of a different form. Indeed it must be since a correction factor is not required for the data sets for air and N_2; hence, the gas *type* influences K. That is, K = 0.9 for CO_2 while K = 1.0 for air and N_2. It is also noted that K must be a function of porosity. The reason for this consideration is that K must be 1, even for CO_2, as porosity approaches 1; therefore, for the CO_2 data sets, K must at least vary from 0.9 to 1.0 for porosities varying from 0.93 to 1.0, respectively. For purposes of this thesis, K can only be interpreted as a factor necessary for good correlation between experimental data and the models. Further testing of a fibrous material at different densities (porosities) is needed to determine the exact nature of K.

While the SPCM is fundamentally a much simpler model than the UCCM, it does well in predicting the effective thermal conductivity for all the data sets obtained in this study. The correlation coefficients for each data set are given in Table 2. The SPCM appears to fall short for the CO_2 at -30°C. This appears to be due to the lack of compensation for contact points in this model. Since the thermal resistance at a contact point increases as temperature and pressure decrease, the effective thermal conductivity predicted by the SPCM is thought to be over predicted at low pressures. The lack of compensation for contact points is affected by pressure more than by temperature. This is noted since there is excellent agreement between the models and experimental data for N_2 at -50°C from medium to high pressure ranges.

7.5 *UCCM Correlation*

The parameters governing the UCCM are also examined for their physical significance to determine whether the values obtained are of the expected order of magnitude. The parameters l_{eff}, ϕ, and h_cA_c are determined by correlation to the reference data set. The effective conduction path length, l_{eff}, is found to be ~0.0042m. This is reasonable since the sample thickness is 0.012m. The angle ϕ is determined to be slightly less than 90°. Initially, this was somewhat disturbing since it was expected to be ≤45° for a material consisting of randomly oriented fibers. However, since the vertical cell can be represented equivalently as shown in Fig. D-1 in Appendix D, then the fibers could be considered to be modeled as if they are oriented on average at 45° with respect to the xy-plane. Imakoma et al. [4] used angles of 11.3° and 45° for ϕ in modeling two different fibrous materials (essentially the same model as the UCCM), but these values were based on intuition. The cell angles for this work are determined from a "best fit" of the reference data. The portion of contact resistance due to h_cA_c is determined to be on the order of 10^{-9} W/°C. This is neglected in the model calculations. Finally, the contribution to radiation, λ_R, at 20°C is found to be ~0.0014 W/m°C which corresponds to an effective emissivity, Σ_T, of ~0.02. Once these parameters are found, they are held fixed since they are considered to be characteristic of the physical structure of the material. The model is then used to determine the degree of accuracy with which it could predict for various other conditions the effective thermal conductivity of Nomex.

The UCCM is in excellent agreement with the experimental data, as shown in Figures 23, 25, and 26, but exhibits a slight difference in the transition region. The same correction factor, K, for the CO_2 conductivity, as in the SPCM, is used in correlating the UCCM to the reference data. The correlation coefficients for the UCCM are compared to the SPCM in Table 2.

Table 2. Correlation coefficients of conduction models corresponding to each data set.

	Air @ 20°C	CO_2 @ 20°C	CO_2 @ 0°C	CO_2 @ -30°C	N_2 @ -50°C
SPCM	0.9985	0.9984	0.9956	0.9158	0.9954
UCCM	0.9973	0.9967	0.9946	0.9685	0.9922

7.6 *Observations*

The experimental data (Tables 3 through 7 and Fig. 20) show the variation in effective thermal conductivity for Nomex as it depends upon fill-gas pressure. At low pressures, the effective thermal conductivity approaches an asymptote where radiation and solid conduction through the fibers and fiber contacts are the only contributors to the effective thermal conductivity of the fibrous material. These two contributions, $\lambda_R + \lambda_F$, are independent of changes in pressure. Again, the effective thermal conductivity approaches an upper limit at higher pressures due to the extremely small mean free path of the gas as compared to the mean distance between fibers such that the gas within the fibrous solid behaves essentially as a free gas. Finally, the central region in which the effective thermal conductivity of a fibrous material changes dramatically is the transition from discrete particle behavior to continuum behavior.

It is evident that the most influential part of the model is due to gas conduction. Unless the gas conductivity is adequately evaluated as a function of temperature and pressure, models can be seriously hindered from reasonably predicting the effective thermal conductivity of fibrous materials, particularly at low pressures (<10 mmHg). Some investigators [1, 2, 3] have neglected the effect of temperature jump in a gas at reduced pressures as discussed in Section 3.2. Others [7, 10, 11] accounted for temperature jump but may have inadequately done so by neglecting the "two-sided" nature of the Maxwellian distribution function. This resulted in gas conductivity representations

that are inaccurate in the transition region. Figure 21 shows the comparison of the conductivity of air at 20°C employing the gas thermal conductivity equations used by several investigators. When the *imperfect* energy transfer of a rarefied gas is not adequately taken into account (along with variations in determining the mean distance between fibers), the transition region drifts to the left as compared to the gas model used in this work. The equation similar to that derived by Lees and Liu [11,12] using the Maxwell moment method was employed for this work.

7.6.1 *Comparison of Models to Experiments*

The SPCM and the UCCM both agreed well with the experimental data as shown by Figs. 22 - 26. The models differed, however, in their predictions at low pressures and temperatures. The UCCM predicted lower than the SPCM for CO_2 at 0°C and -30°C (compare Figs. 24 and 25) and for N_2 at -50°C (Fig. 26) at lower pressures. Regrettably, no data were obtained at low temperatures *and* low pressures due to the instability of the guard heater controller at those conditions. Both models were benchmarked against the reference data and both agreed well over the entire range of pressures. However, the fiber contact resistance of the UCCM changes with pressure and temperature, thus accounting for the continual reduction in the prediction of effective thermal conductivity as the pressures and temperatures decrease. The difference in the model predictions is due to the modeling of fiber contact resistance in the UCCM. Using the parameters previously given for the UCCM, $\lambda_{s,eff}$ varies from 0.13 W/m°C at ambient conditions to ~0.057 W/m°C in vacuum conditions. This is less than half the actual solid conductivity, λ_s, of 0.13 W/m°C.

Figure 22 shows the correlation between the Series/Parallel Conduction Model and

experimental data for air and CO_2 at 20°C. It is noted that both curves converged to the same value of effective thermal conductivity as the pressure decreases. This is expected since, as the pressure is reduced, there are fewer molecules in the chamber; thus, with fewer molecules, there is less influence on the *type* of gas involved in the heat transfer.

Figure 23 shows the comparison between the Unit Cell Conduction Model and the Series/Parallel Conduction Model with the experimental data for air at 20°C. Both models predict with essentially the same accuracy for the data sets at 20°C. The difference was within the uncertainty of the measurements and, therefore, considered negligible.

Figure 24 shows the correlation between the Series/Parallel Conduction Model and experimental data for CO_2 at 20, 0, and -30°C. It is noted that the curves did not converge to the same value of effective thermal conductivity as the pressure is reduced. This is expected since the curves represent the effective thermal conductivity of the material at different temperatures. Although the solid conductivity, λ_s, is assumed to be relatively constant for the temperature range considered, the contribution to heat transfer due to radiation and gas conduction decreases as temperature decreases.

Figure 25 shows the correlation between the Unit Cell Conduction Model and experimental data for CO_2 at 20, 0, and -30°C. It is noted again that the curves do not converge to the same value of effective thermal conductivity. This was expected as with the SPCM since the curves represent the effective thermal conductivity of the fibrous material at different temperatures. However, the UCCM consistently predicts lower than the SPCM for the data sets obtained at temperatures < 20°C at low pressures. This is due to the modeling of fiber contact points within the UCCM. The thermal contact resistance between fibers increases as the temperature and pressure decreases; therefore, the effective thermal conductivity of the solid fiber, $\lambda_{s,eff}$, decreases. Hence, as $\lambda_{s,eff}$ decreases, the

effective thermal conductivity of the fibrous material also decreases.

Figure 26 shows the correlation between the Series/Parallel Conduction Model, Unit Cell Conduction Model, and experimental data for N_2 at -50°C. The SPCM yielded a 99.5% correlation with λ_s = 0.13 W/m°C. This curve aided in the assumption that the solid fiber conductivity, λ_s, was relatively constant over the temperature range considered. The UCCM also predicts well (99.2% correlation) the effective thermal conductivity at this low temperature for higher pressures. However again, the UCCM predicts lower than the SPCM at low pressures. This is assumed to be due to the aforementioned reasons stated for Fig. 25.

Figure 27 shows the comparison between the Series/Parallel Conduction Model and the Unit Cell Conduction Model in air and CO_2 as a function of temperature at 100 kPa. The plot for N_2 looks essentially the same as that for air so the data point for N_2 near ambient conditions is shown. The increase in effective thermal conductivity as temperature increases is due solely to gas conduction and radiative conduction (and in the UCCM increased thermal conduction across fiber contact points) since λ_s is assumed constant.

7.6.2 *Comparison of Effects of Different Mechanisms*

The following figures are given to support some of the conclusions derived. The essential difference between the SPCM and the UCCM is the modeling of contact resistance at fiber contact points within the fibrous material. Illustrations of the effective thermal conductivity of the solid fiber, $\lambda_{s,eff}$, and the gas conductivity at or near the contact point are given as a function of fill-gas pressure. As a consequence of the

difference in the two models at vacuum conditions, the predictions of radiative conductivity differ.

Figure 28 shows the effective thermal conductivity of the solid fiber used for the UCCM as a function of temperature and pressure (eqn.(19)). At ambient pressures, the effective thermal conductivity of the solid fiber, $\lambda_{s,eff}$, is equal to the actual solid fiber conductivity, λ_s. As the gas pressure is reduced, $\lambda_{s,eff}$ approaches values less than λ_s for different fill-gases and temperatures. This is attributed to the lower predictions of effective thermal conductivity at low pressures and temperatures than that predicted by the SPCM.

Figure 29 shows the thermal conductivity of a gas at a fiber contact point as a function of temperature (eqn.(20)). The contribution by gas conductivity at the contact point is negligible for pressures less than 100 Pa. This term contributes to the increased contact resistance as pressure decreases.

Figure 30 shows the comparison between the radiative conductivity predictions of the Series/Parallel Conduction Model and the Unit Cell Conduction Model as a function of temperature. The difference is due to the different predictions of effective thermal conductivity of the fibrous material at rarefied conditions. The UCCM predicts a greater contribution to radiation than the SPCM. This was expected since both models agreed at rarefied conditions for air at 20°C, but the UCCM predicts a lower effective thermal conductivity than the SPCM for lower temperatures at rarefied conditions.

Table 3. Effective thermal conductivity as a function of air pressure.

Material: Nomex
Fill-gas: air
Mean temperature: 20°C

Pressure (mmHg)	Effective Thermal Conductivity (W/m°C)
0.0052 ±1.9%	0.00417 ±3.4%
0.102 ±0.10%	0.00691 ±3.0%
0.310 ±0.03%	0.0111 ±2.9%
0.93 ±0.01%	0.0164 ±2.9%
2.51 ±3.9%‡	0.0227 ±2.9%
9.90 ±1.0%	0.0283 ±2.9%
28.65 ±0.34%	0.0308 ±2.9%
139.5 ±0.07%	0.0325 ±2.9%
731.6 ±0.01%	0.0336 ±2.9%

Table 4. Effective thermal conductivity as a function of CO_2 pressure.

Material: Nomex
Fill-gas: CO_2
Mean temperature: 20°C

Pressure (mmHg)	Effective Thermal Conductivity (W/m°C)
0.0045 ±2.2%	0.00389 ±3.4%
0.057 ±0.18%	0.00544 ±3.2%
0.24 ±0.04%	0.0086 ±3.0%
0.90 ±0.01%	0.0136 ±2.9%
3.1 ±3.2%	0.0178 ±2.9%
10.0 ±1.0%	0.0202 ±2.9%
42.1 ±0.23%	0.0219 ±2.9%
116.9 ±0.08%	0.0227 ±2.9%
651 ±0.01%	0.0231 ±2.9%

‡ The sudden jump in uncertainty was due to the change from using in the vicinity of 1 mmHg the Ruska pressure gage to the 1 torr barotron.

Table 5. Effective thermal conductivity as a function of CO_2 pressure.

Material: Nomex
Fill-gas: CO_2
Mean temperature: 0°C

Pressure (mmHg)	Effective Thermal Conductivity (W/m°C)
0.008 ±1.3%	0.00355 ±3.5%
0.13 ±0.08%	0.00633 ±3.1%
0.61 ±0.02%	0.0115 ±2.9%
2.00 ±4.9%	0.0151 ±2.9%
10.7 ±0.92%	0.0185 ±2.9%
67.4 ±0.15%	0.0202 ±2.9%
597.0 ±0.02%	0.0214 ±2.9%

Table 6. Effective thermal conductivity as a function of CO_2 pressure.

Material: Nomex
Fill-gas: CO_2
Mean temperature: -30°C

Pressure (mmHg)	Effective Thermal Conductivity (W/m°C)
1.06 ±0.01%	0.0120 ±3.7%
1.33 ±7.4%	0.0125 ±3.7%
3.55 ±2.8%	0.0149 ±3.6%
5.49 ±1.8%	0.0157 ±3.6%
10.17 ±0.97%	0.0164 ±3.6%
28.20 ±0.35%	0.0174 ±3.6%
97.75 ±0.10%	0.0184 ±3.6%
428.4 ±0.02%	0.0189 ±3.6%

Table 7. Effective thermal conductivity as a function of N_2 pressure.

Material: Nomex
Fill-gas: N_2
Mean temperature: -50°C

Pressure (mmHg)	Effective Thermal Conductivity (W/m°C)
1.02 ±0.01%	0.0157 ±3.6%
1.52 ±6.5%	0.0180 ±3.6%
2.78 ±3.5%	0.0211 ±3.6%
4.80 ±2.1%	0.0228 ±3.6%
9.54 ±1.0%	0.0245 ±3.6%
27.7 ±0.35%	0.0261 ±3.6%
54.3 ±0.18%	0.0270 ±3.6%
97.4 ±0.10%	0.0274 ±3.6%

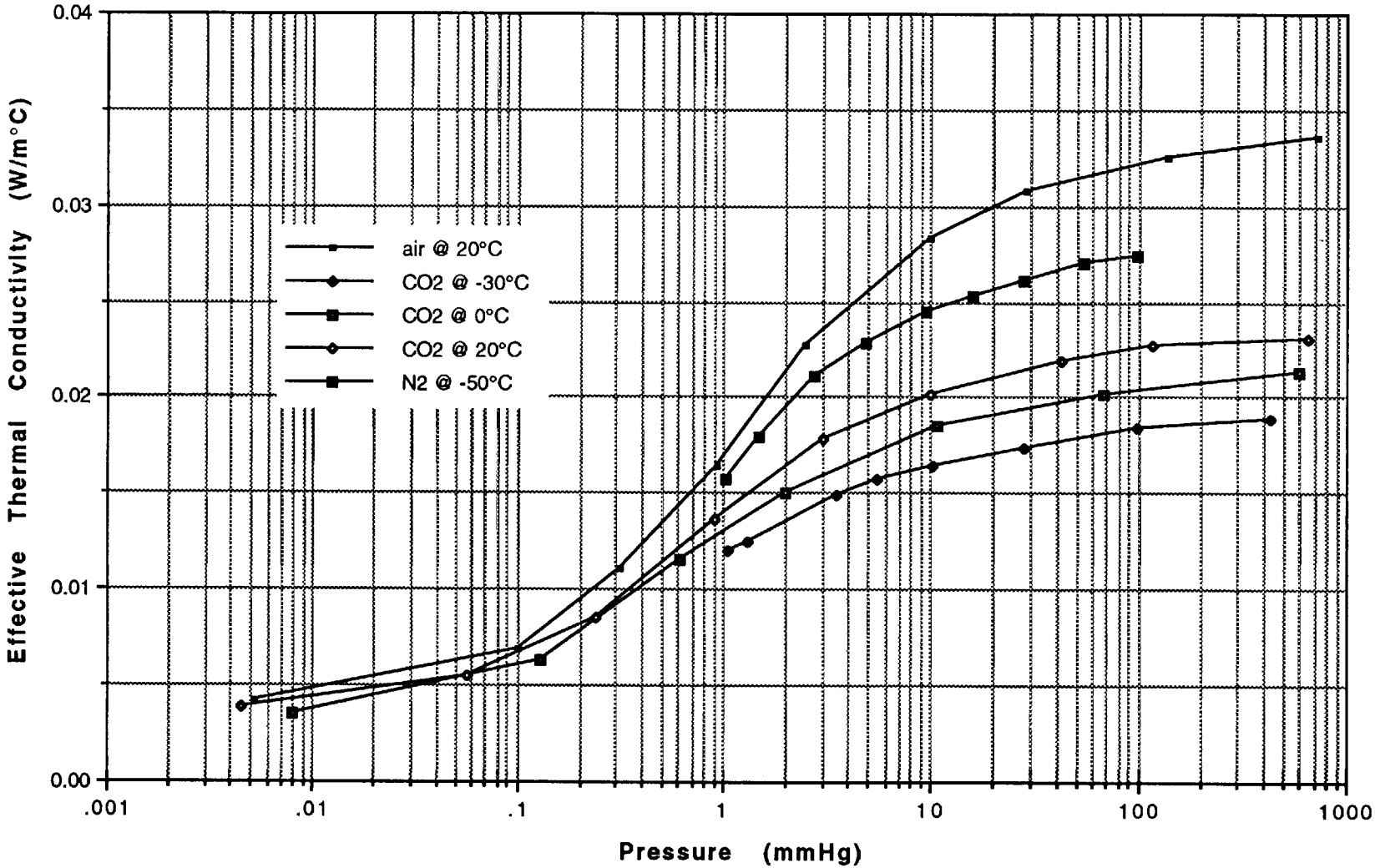

Figure 20. Effective thermal conductivity of Nomex as a function of fill-gas pressure (experimental data)

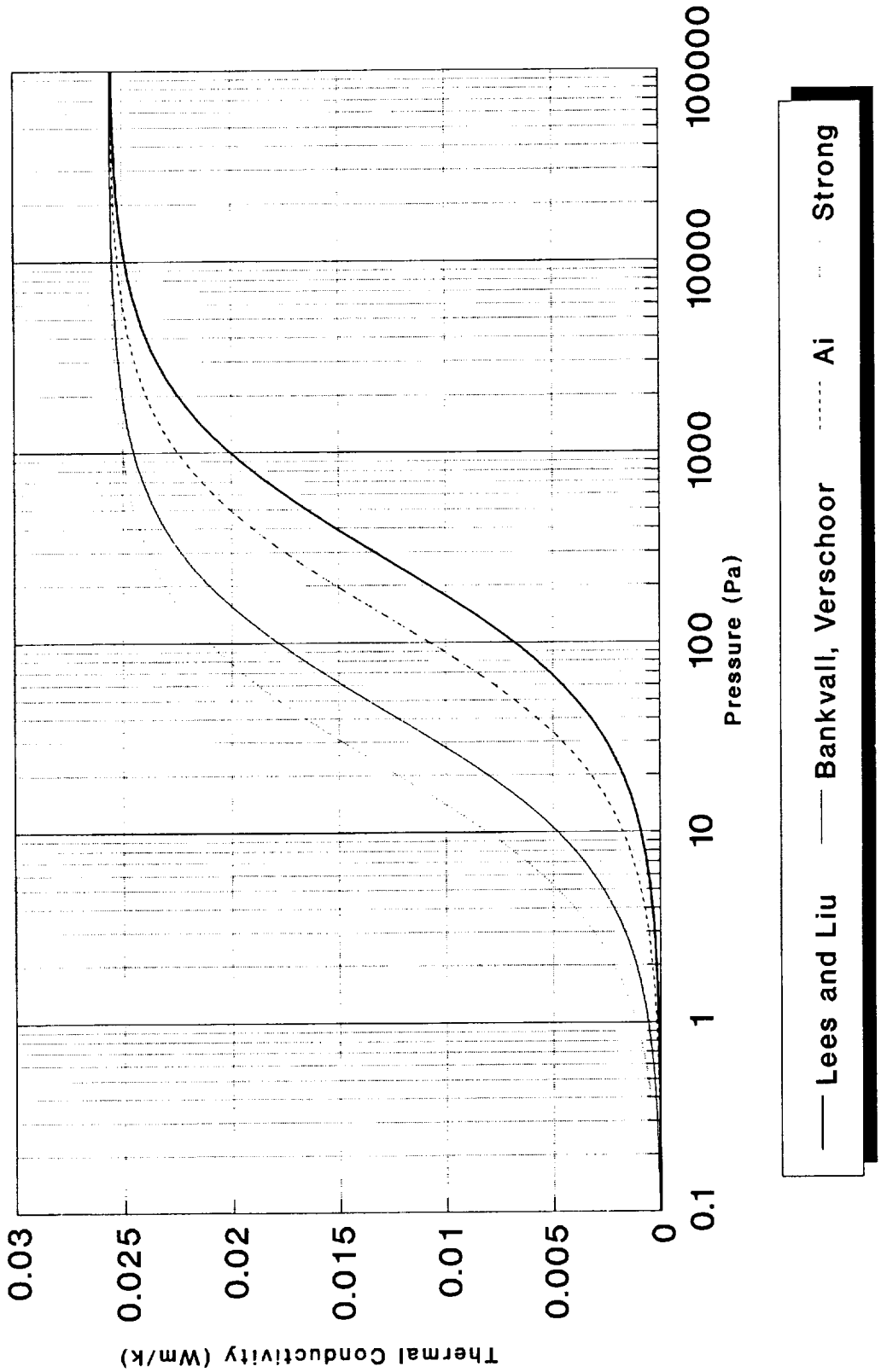

Figure 21. Thermal conductivity of air at 20 degC

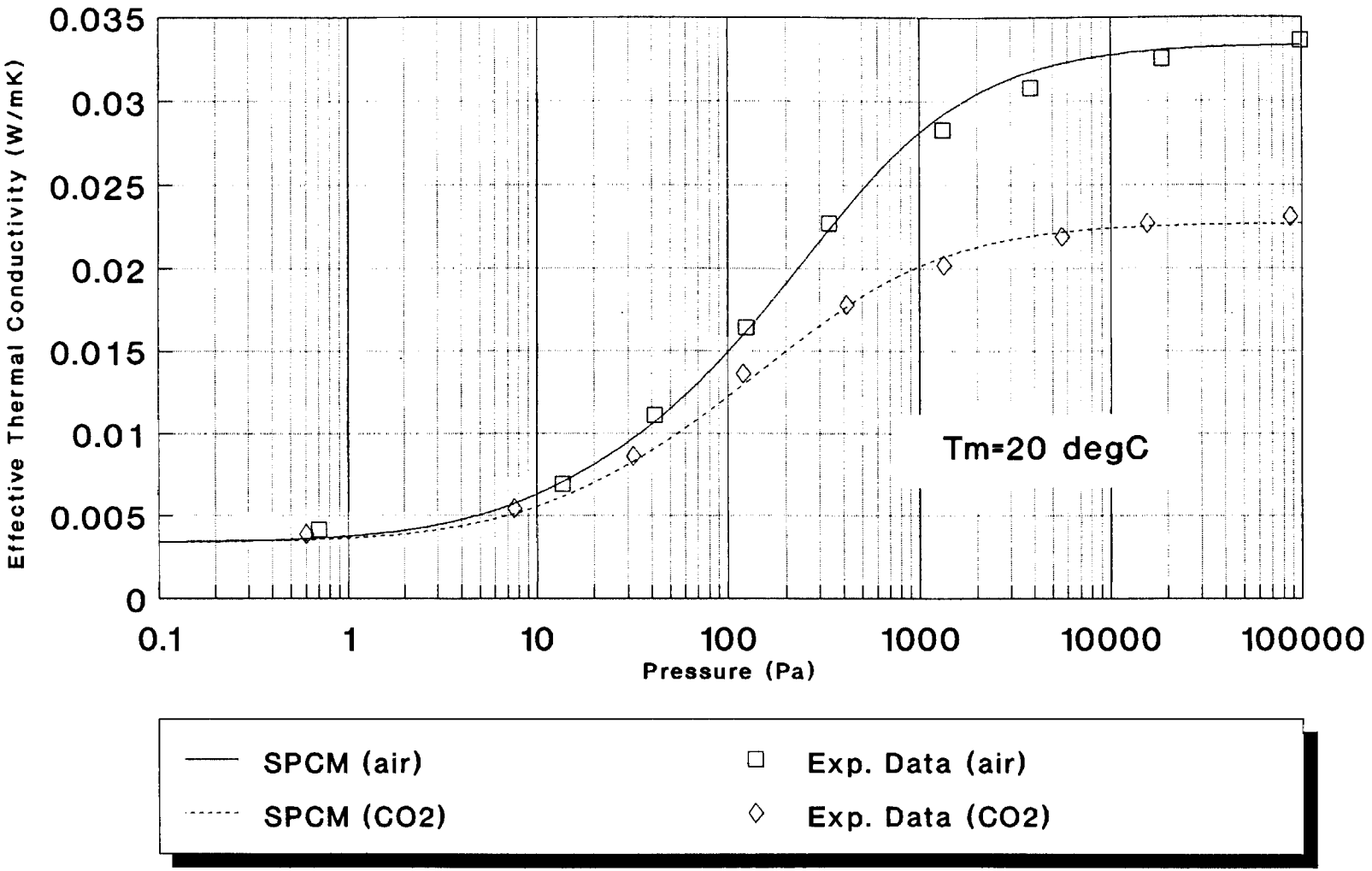

Figure 22. Effective thermal conductivity of Nomex in air and CO2

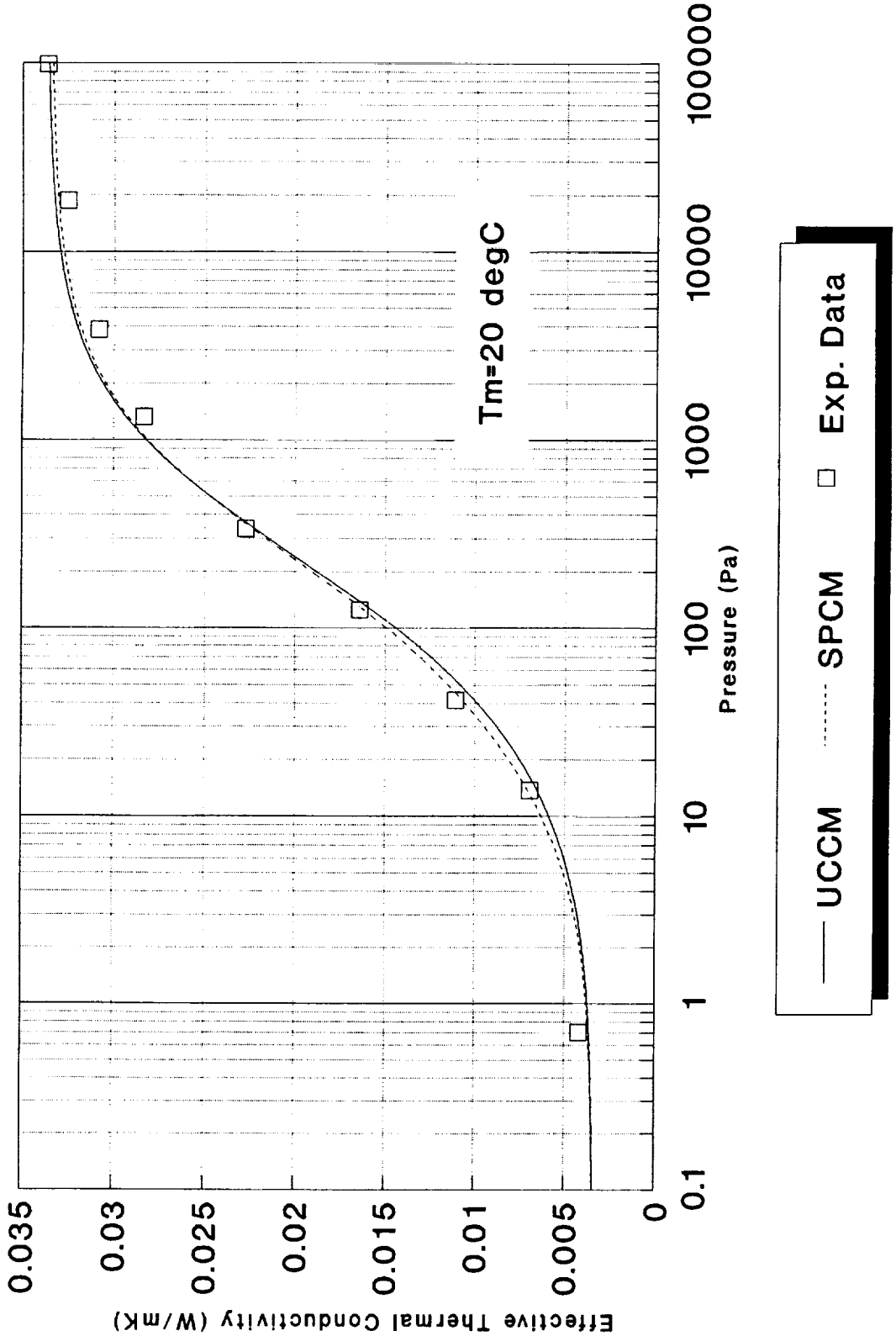

Figure 23. Effective thermal conductivity of Nomex in air

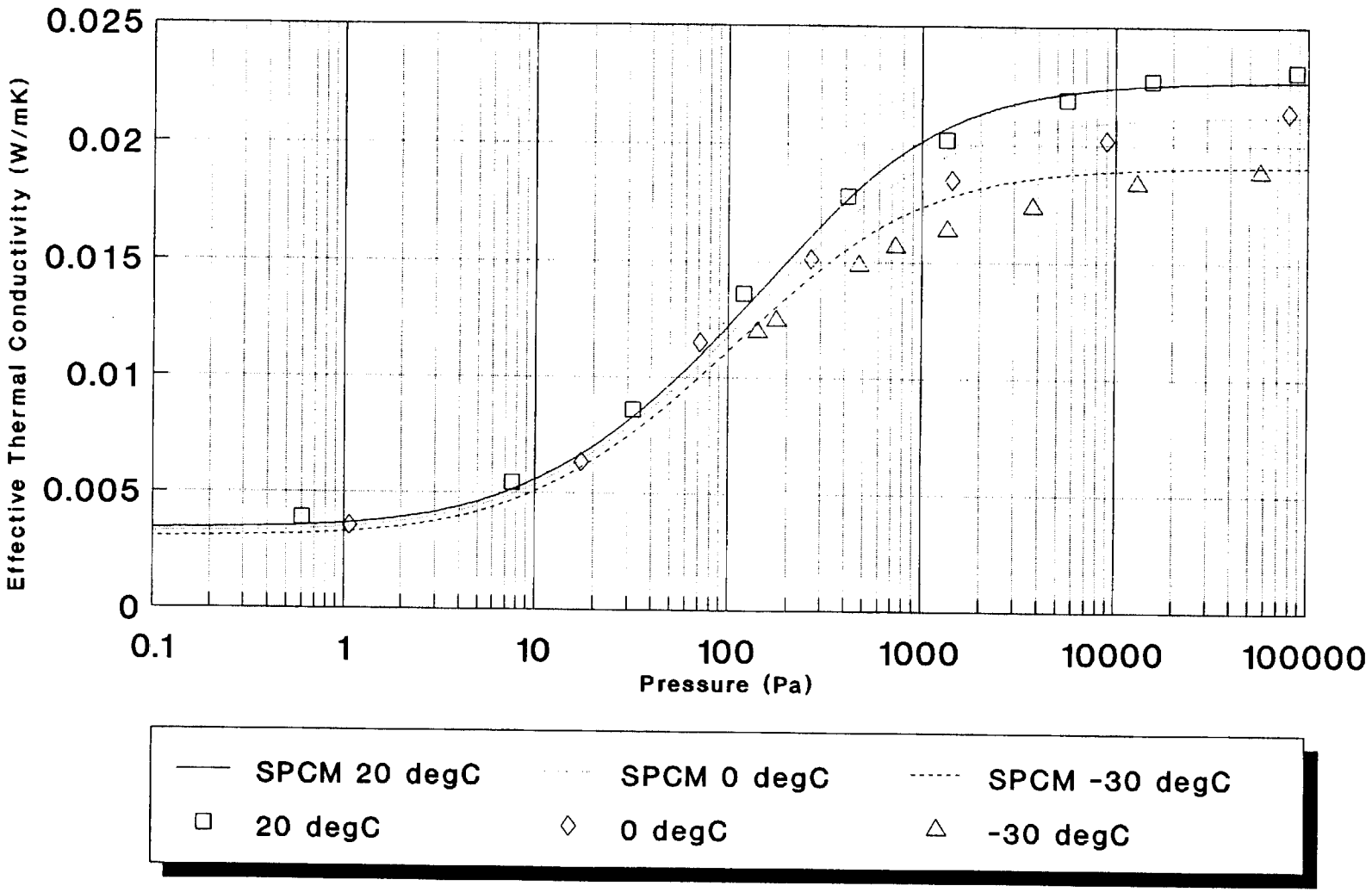

Figure 24. Effective thermal conductivity of Nomex in carbon dioxide atmosphere

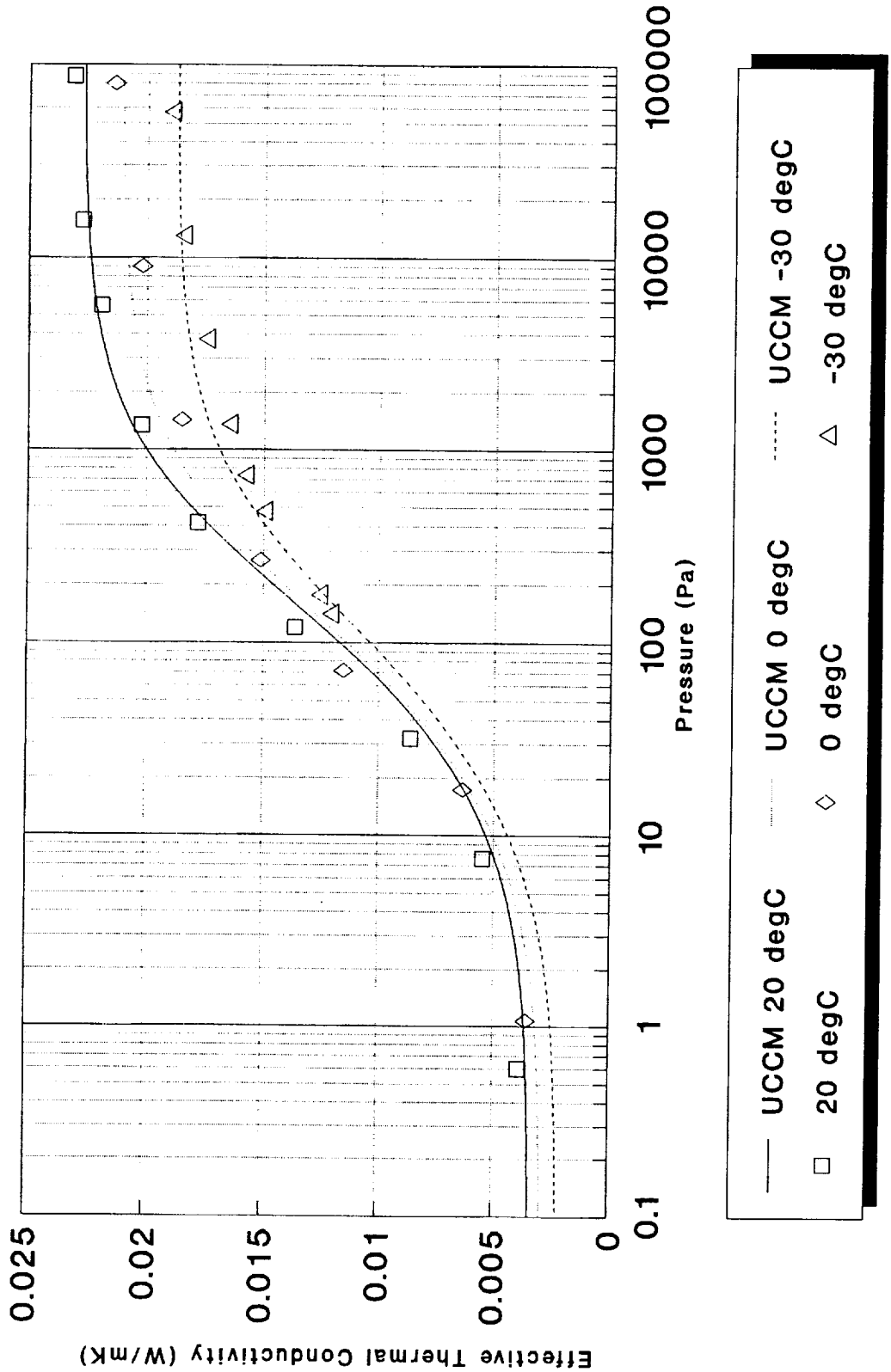

Figure 25. Effective thermal conductivity of Nomex in carbon dioxide atmosphere

C-2

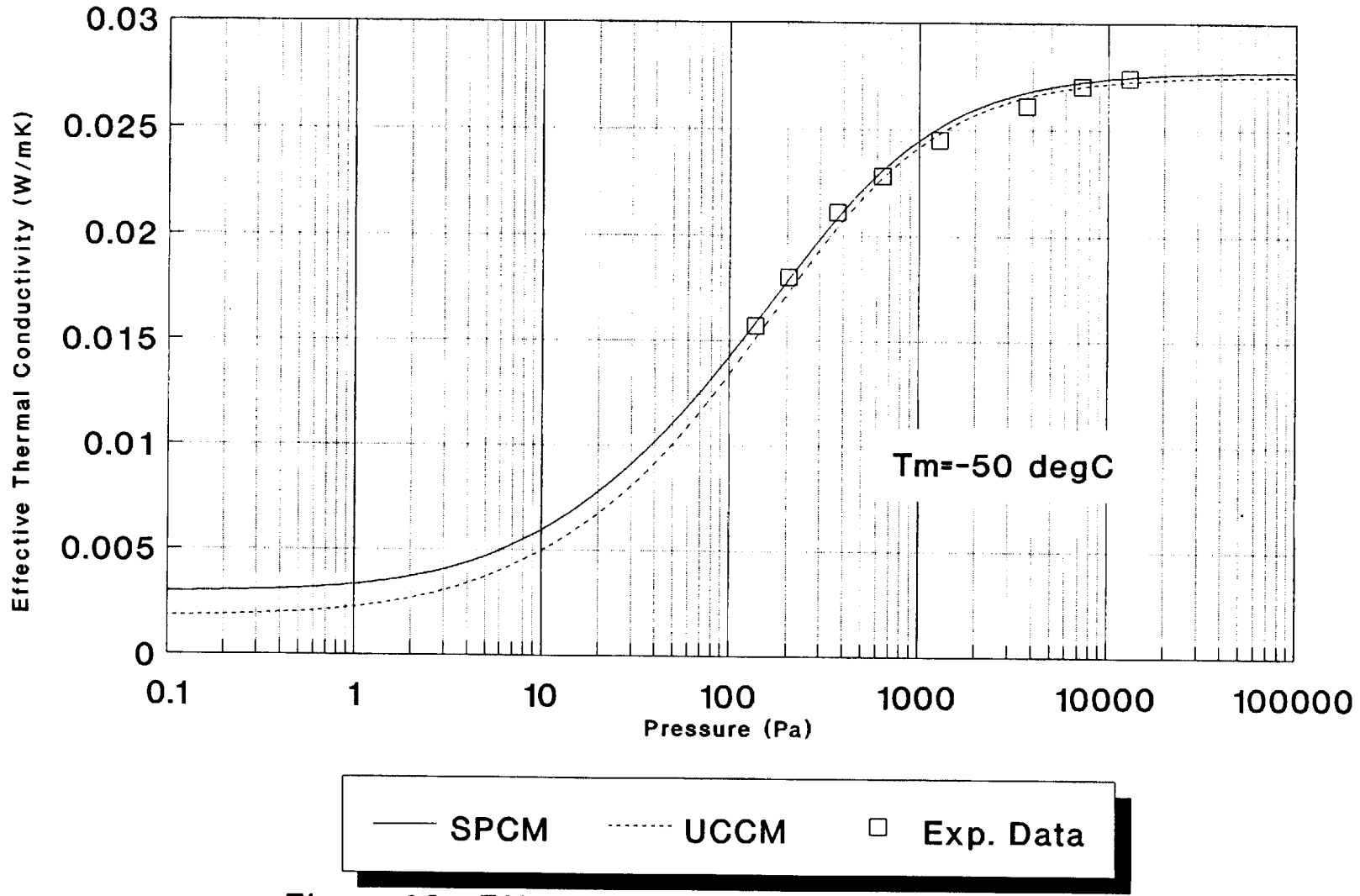

Figure 26. Effective thermal conductivity of Nomex in nitrogen atmosphere

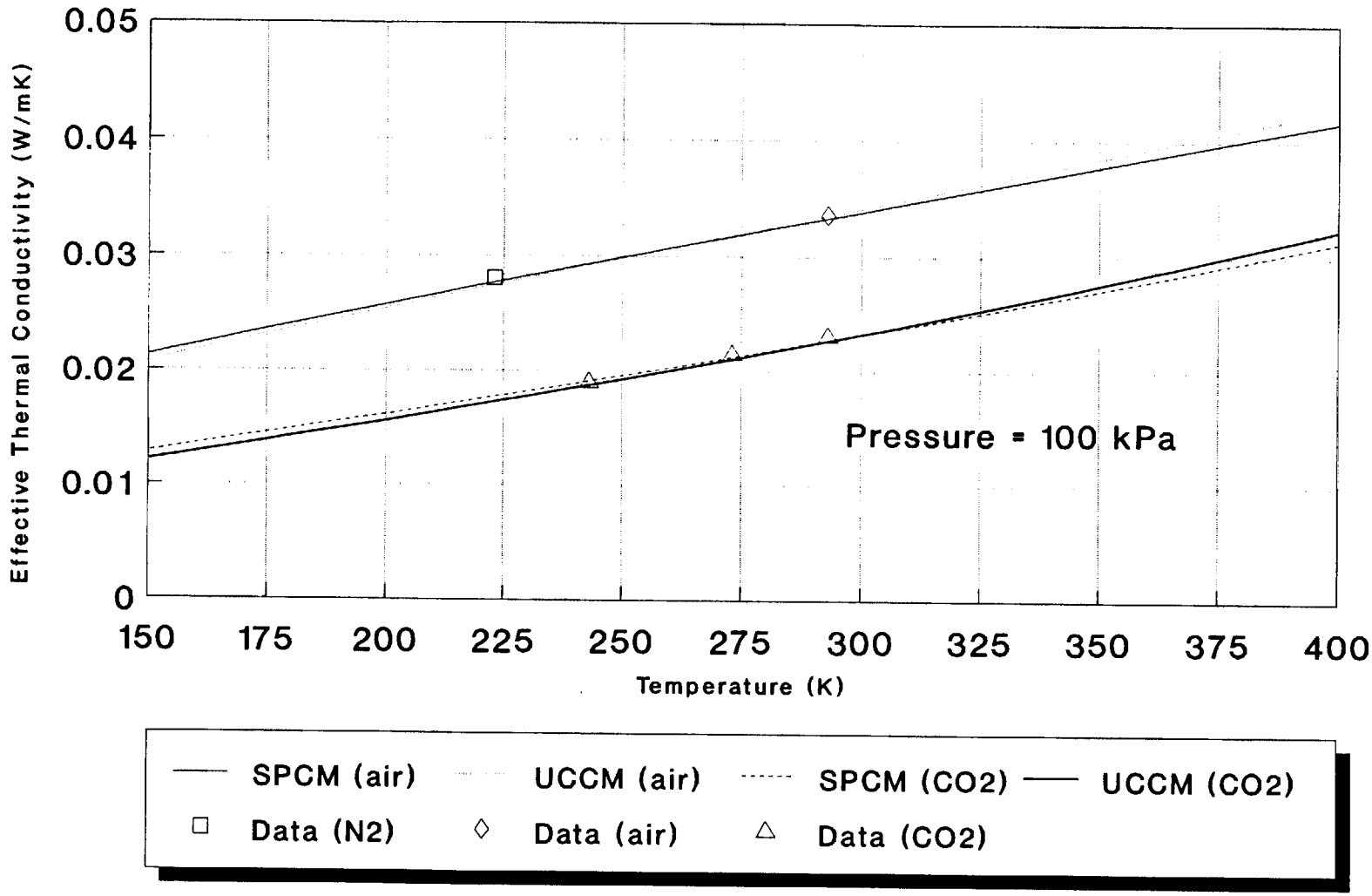

Figure 27. Effective thermal conductivity of Nomex as a function of temperature

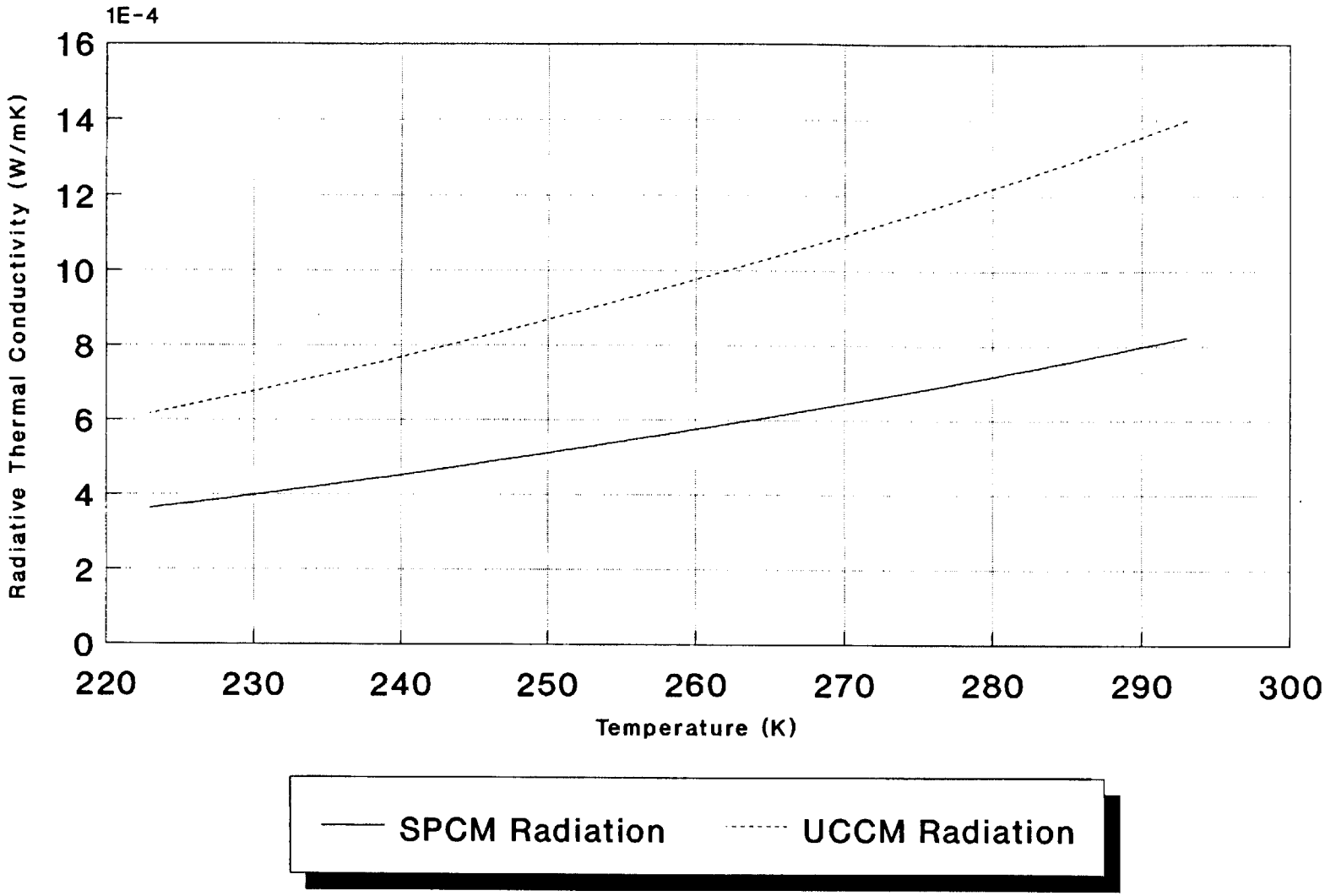

Figure 28. Thermal conduction due to radiation

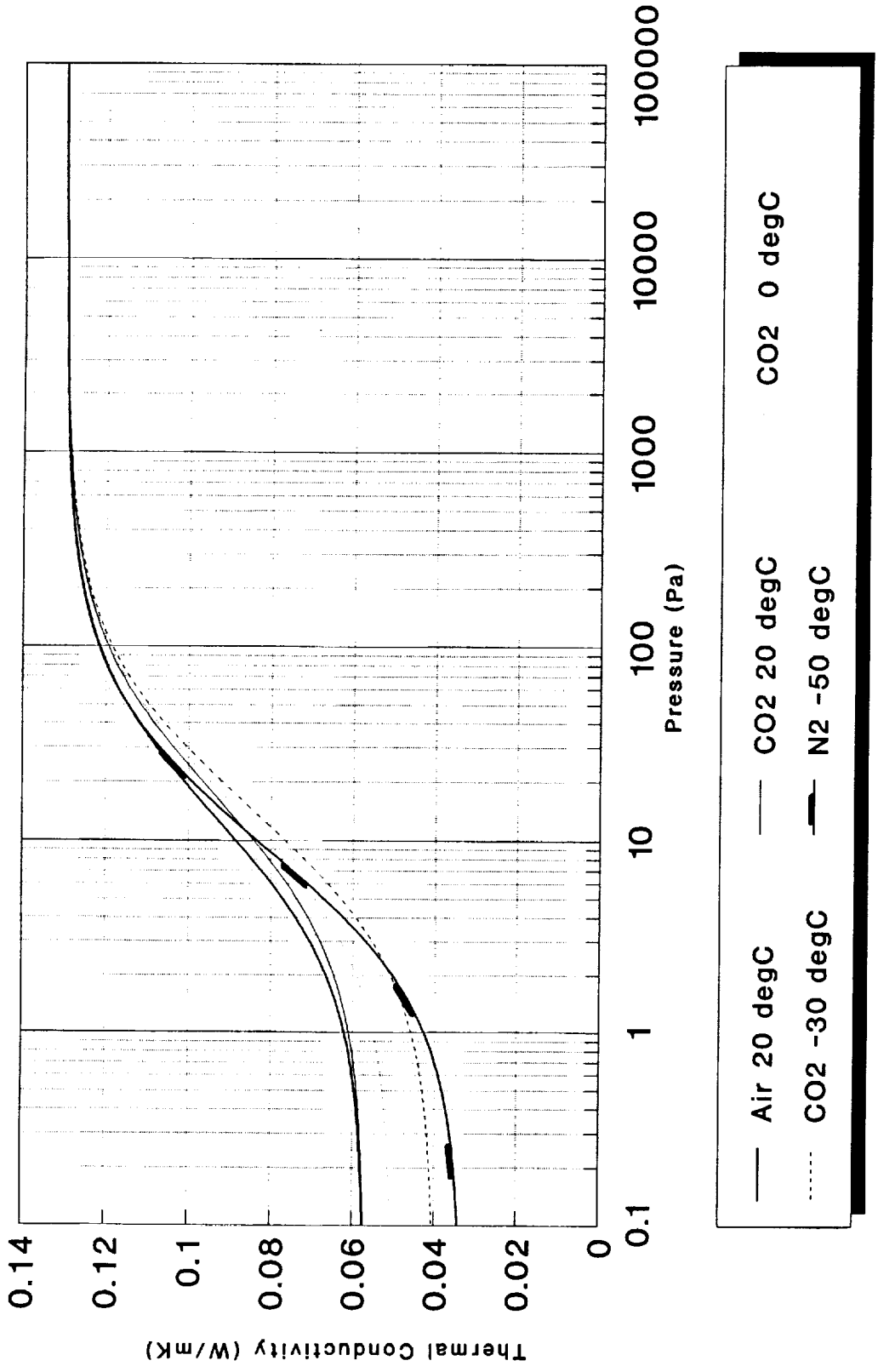

Figure 29. Effective thermal conductivity of solid fiber

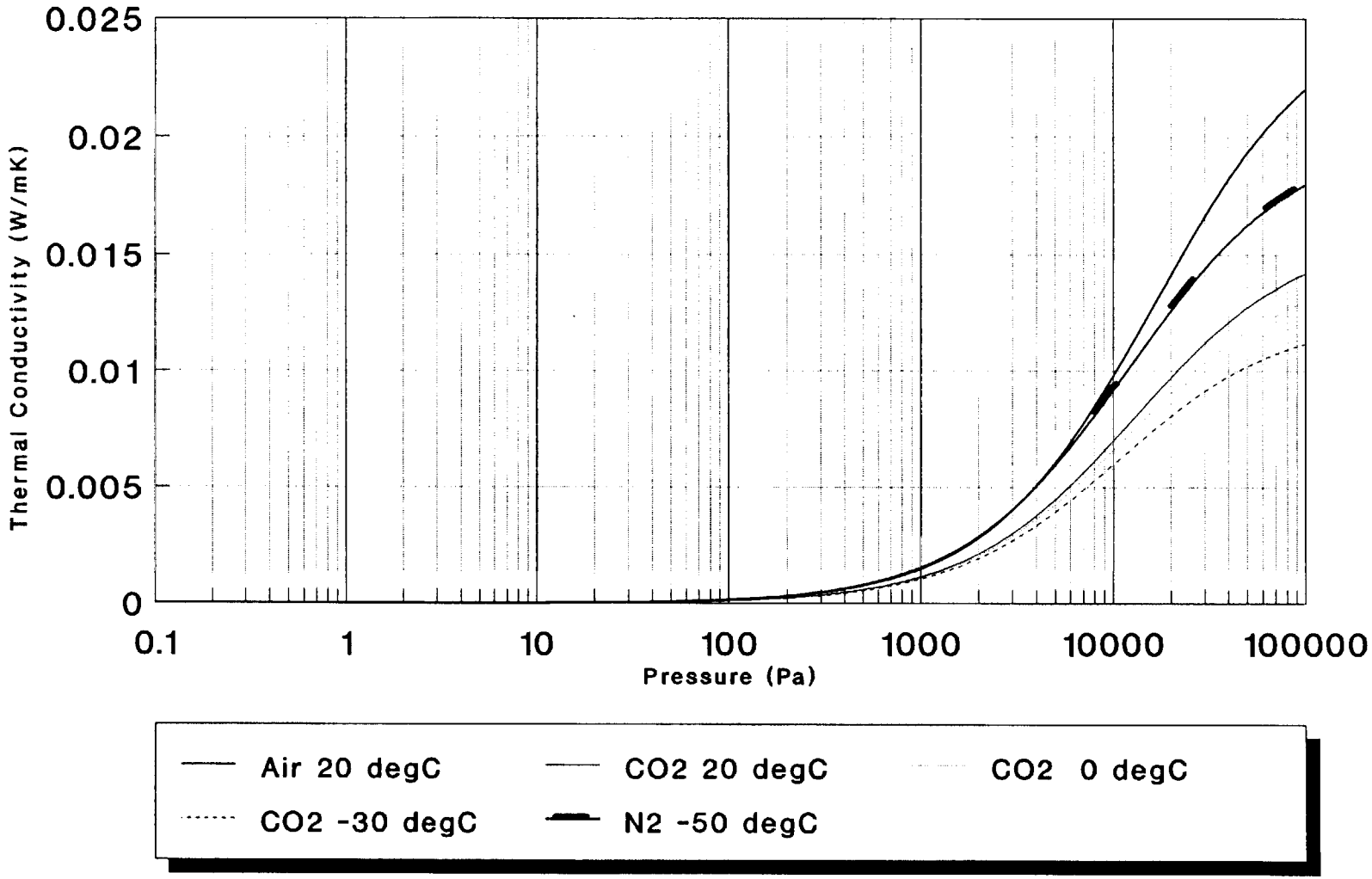

Figure 30. Thermal conductivity of gas at fiber contact point

Chapter 8 *Summary and Conclusions*

The objective of this thesis is to determine the influence of fill-gas pressure on the performance of random-fiber thermal insulation for various gas types. As an adjunct to this, a mathematical model is developed to predict the effective thermal conductivity of such a class of insulation.

Experiments are conducted for Nomex using a double-sided guarded hot plate heater apparatus. Data are obtained for various temperatures and fill-gas pressures; i.e., the temperature is held constant while several test points are obtained over the pressure range from vacuum conditions (~10^{-4} Pa) to atmospheric (101 kPa).

Two models are developed: the Series/Parallel Conduction Model (SPCM) and the Unit Cell Conduction Model (UCCM). Both of these models require modeling of conductive and radiative effects. A significant contribution of this thesis is an improvement in the representation of the gas conductivity at reduced pressures. The gas conduction is found to be a crucial component in accurately predicting the effective thermal conductivity of a fibrous material. The accuracy of the models is dominated by the gas conductivity contribution.

Both the SPCM and the UCCM are effective in predicting the effective thermal conductivity of Nomex as a function of temperature over a range of pressures. The structural parameters specific to each model are determined based on the correlation to a reference data set. With the parameters held constant, the models do relatively well in adjusting the effective thermal conductivity as the atmosphere changes. It is noted that the UCCM predicts lower values of effective thermal conductivity at lower pressures than that predicted by the SPCM. This is due to the modeling of contact resistance at fiber contact

points within the UCCM. However, with the increased uncertainty in the measured value of effective thermal conductivity at lower pressures and temperatures, it is difficult to determine if one model is more accurate than the other. Based on the CO_2 data obtained at -30°C, the UCCM seems to be more adaptable to changes in atmospheres.

The SPCM proved useful especially at higher pressures. It is beneficial due to its simplicity and ease of implementation. The UCCM, however, is more complex and requires more effort in determining the structural parameters characteristic of the fibrous material being modeled. Both models are useful, but the UCCM may give slightly more accurate results for low temperature, low pressure environments.

It should be noted that both models require a correction factor, K, for CO_2. While the exact nature of K could not be determined, it is thought that it depends upon the structural nature of the insulation as well as the structure of the gas molecule.

Thermal properties may be well known for some fibrous materials under certain atmospheric conditions. It may be important to determine the influence of the atmospheric environment on heat transfer through these materials. In those cases, the models can provide a way for correlating the existing data to obtain certain structural parameters characteristic to the material. Then, by changing the gaseous medium, temperature and/or the pressure within the model, one could determine the adjusted thermal conductivity of the same material when subjected to the new environment. Based on the excellent comparisons between the models and experimental data, it should be possible to apply one or both of the models to the prediction of thermal performance of other insulation/fill-gas combinations of the random-fiber class as long as the structural parameters can be found. An obvious application could be for a low pressure, low temperature CO_2 environment like that of the Martian atmosphere.

References

[1] Bankvall, Claes G., "Heat Transfer in Fibrous Materials." National Swedish Building Research, Stockholm, Sweden, 1972.

[2] Strong, H. M., Bundy, F. P., and Bovenkerk, Flat Panel Vacuum Thermal Insulation, Journal of Applied Physics, v31 n 1, 1960, pp 39-50.

[3] Verschoor, J. D., Greebler, P., "Heat Transfer by Gas Conduction and Radiation in Fibrous Insulations," American Society of Mechanical Engineers - Transactions, v 74 n 6, 1952, pp 961 - 968.

[4] Imakoma, H., Sang, H. S., Miyoshi, K., and Okazaki, M., "Effective Thermal Conductivity of Fibrous Insulations," Japanese Research, v 19 n 7, 1990, pp 689-696.

[5] Imakoma, H., Sang, K., and Okazaki, M., "The Effective Thermal Conductivity of Fibrous Insulations," International Chemical Engineering, v 30 n 4, Oct.1990, pp 738-746.

[6] Smith, D. R., Dube W. P., and Filla, B. J., "Automated Low-Temperature Guarded Hot Plate for Measuring Apparent Conductivity," Insulation Materials: Testing and Applications, 2nd Volume, ASTM STP 1116, R. S. Graves and D. C.Wysocki, Eds., American Society for Testing and Materials, Philadelphia, 1991.

[7] Kennard, E. H., Kinetic Theory of Gases, McGraw-Hill Book Company, Inc., New York, 1938, 1st ed., pp 311-327.

[8] Smoluchowski, M. von, Akad. Wiss. Wien., v 107, 1889, p 304; v 108, 1899, p 5.

[9] Knudsen, M., Kinetic Theory of Gases, Methuen and Company, Ltd., London, England, 1934.

[10] Dickins, B. G., "The Effect of Accommodation on Heat Conduction through Gases," Proc. Royal Soc., London A143, 1934, pp 517-540.

[11] Welander, P., "Heat Conduction in a Rarefied Gas: the Cylindrically Symmetrical Case," Arkiv Fysik, v 7, 1954, pp 555-564.

[12] Lees, Lester and Liu, Chung-Yen, "Kinetic-Theory Description of Conductive Heat Transfer from a Fine Wire," The Physics of Fluids, v 5 n 10, Oct.1962, pp 1137-1148.

[13] Liu, Chung-Yen and Lees, Lester, "Kinetic Theory Description of Plane Compressible Couette Flow," Advances in Applied Mechanics, Academic Press, New York, 1961, pp 391-428.

[14] Ai, D. K., "Cylindrical Couette Flow in a Rarefied Gas According to Grad's Equations," GALCIT Hypersonic Research Project, Memorandum No.56, 1960.

[15] Yoshida, K., "Nippon Kagaku Kaishi," Journal of Chemistry Society of Japan, v 67, 1946, p 9.

[16] *, "Standard Test Method for Steady-State Heat Flux Measurements and Thermal Transmission Properties by Means of the Guarded-Hot-Plate Apparatus," Annual Book of ASTM Standards, v 4.06, 1989, p 17.

[17] Rennex, Brian., "Error Analysis for the National Bureau of Standards 1016 mm Guarded Hot Plate," The National Bureau of Standards, Washington D.C., Feb.1983.

[18] Woodside, W., "Deviations from One-Dimensional Heat Flow in Guarded Hot Plate Measurements," Review of Scientific Instruments, RSINA, Vol.28, 1957, p 1933-1937.

[19] Hahn, M. H., Robinson, H. E., and Flynn, D. R., "Robinson Line-Heat-Source Guarded Hot Plate Apparatus," Heat Transmission Measurements in Thermal Insulations, ASTM STP 544, American Society Testing and Materials, 1974, p 167-192.

[20] *, "Properties of Nomex® Aramid Filament Yarns," Du Pont Technical Information, Bulliten NX-17, December 1981.

[21] Williams, S. D., and Curry, D. M., "Prediction of Rigid Silica Based Insulation Conductivity," NASA Technical Paper 3276, National Aeronautics and Space Administration, Houston, Texas, 1993.

[22] Lienhard, John H., A Heat Transfer Text Book, Prentice-Hall, Inc. Englewood Cliffs, New Jersey, 1987, p 599-601.

Appendix A Thermal Conductivity of Air, CO_2, and N_2 at Ambient Pressure

Figure A-1 shows the curve fit for the thermal conductivity of air, CO_2, and N_2 at atmospheric pressure over a range of temperatures. This was used for $\lambda_{g\,ref}$ in eqn.(114a). The data was obtained from Lienhard [22].

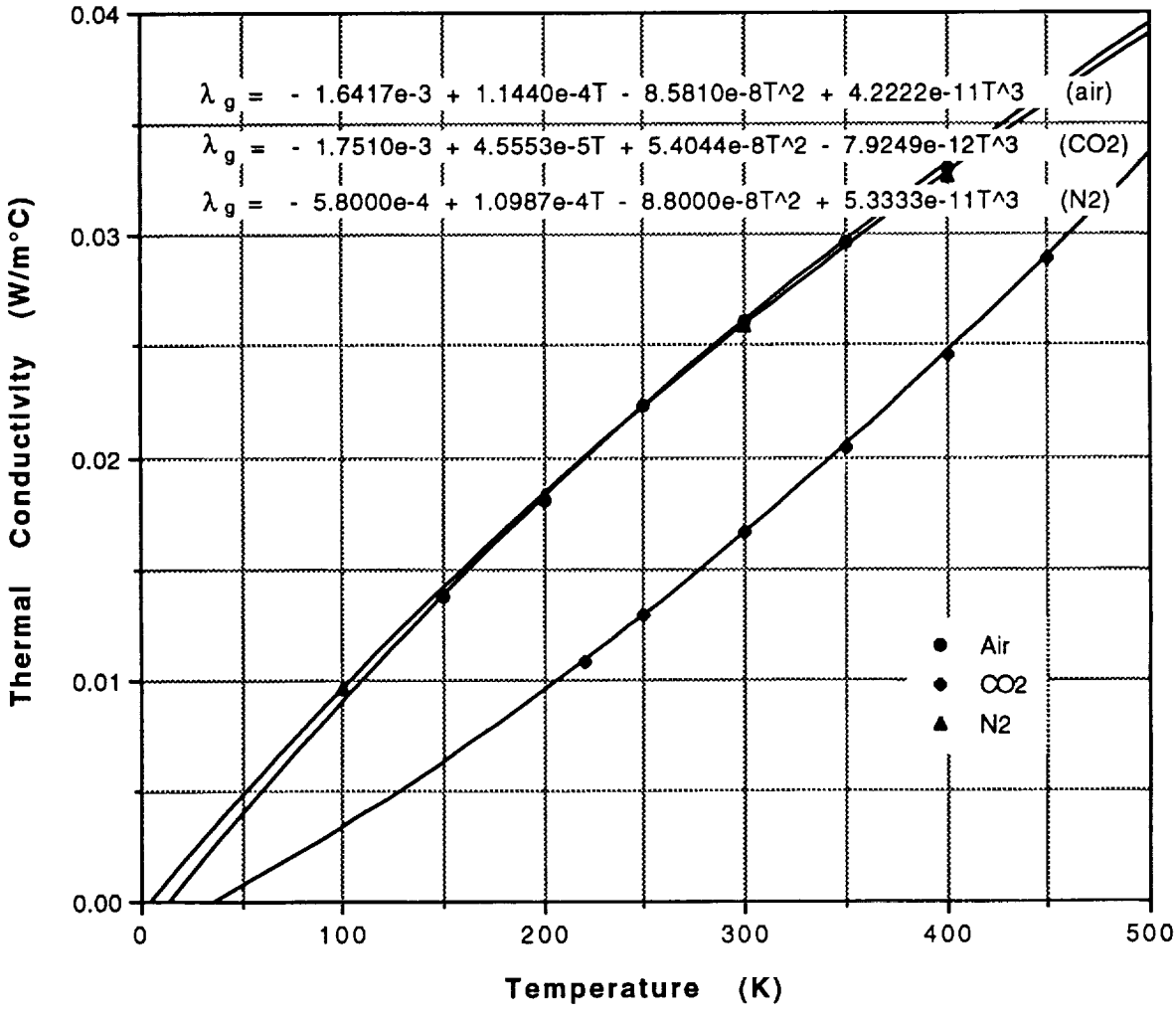

Figure A-1. Gas thermal conductivity

Appendix B Knudsen Number as a Function of Pressure

Figure B-1 shows the Knudsen number, Kn, based on the mean distance between fibers at 20°C over a range of pressures.

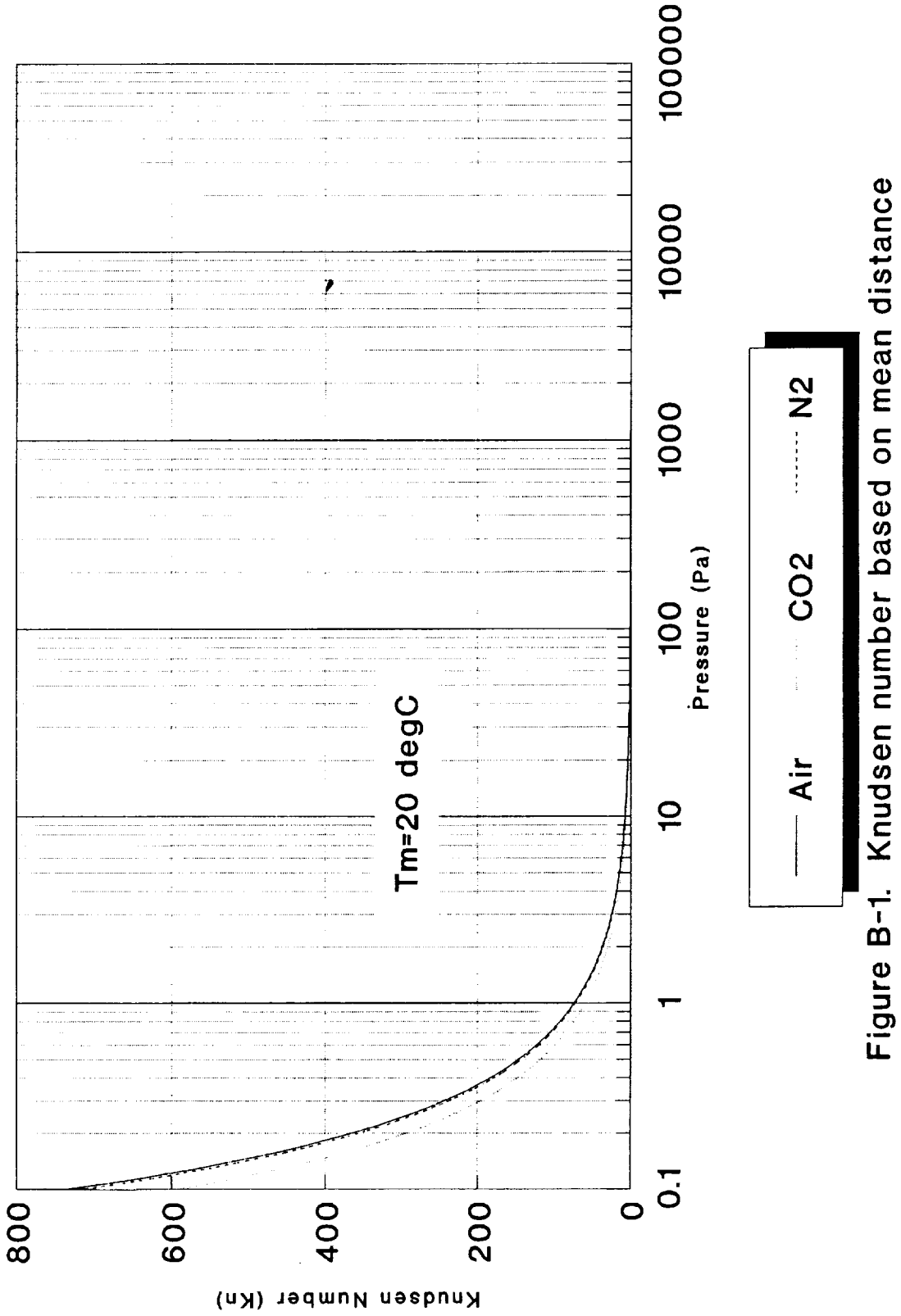

Figure B-1. Knudsen number based on mean distance between fibers

Appendix C Method for Obtaining Maximum Compressed Density

The maximum density of the fibrous material is determined by compressing the material to some assumed maximum. The porosity is determined for the new compressed configuration. From the new calculated porosity, an estimate of the number of fibers per unit distance within one layer is evaluated from [1]

$$N = \frac{4}{\pi} \frac{(1 - \varepsilon)}{D} , \qquad \text{(C-1)}$$

where N = the number of fibers in a layer per unit length,

D = the diameter of the fibers, and

ε = the porosity of the compressed material.

An estimated total contact area is determined based on the number of contact points along each fiber and contact area. Assuming that the tensile strength of Nomex fibers is approximately equal to the compressive strength of the fibers, a corresponding force can be calculated which will yield the maximum pressure possible without fracturing the fibers. If this force does not correspond to the pressure which yielded the compressed configuration, additional load is applied, and the process is repeated.

Appendix D Equivalent Vertical Cell Representation

Figures D-1 through D-3 differ only by rotation about the y-axis. Figure D-2 is the same as Fig. 6 shown in Section 2.3 and was used to derive the effective thermal conductivity of a vertical cell, λ_v. Formally, the vertical cell should look as shown in Fig. D-1. However, if λ_{v1} is associated with the effective thermal conductivity of Fig. D-2 and λ_{v2} with Fig. D-3, then the square of the effective thermal conductivity of the vertical cell can be expressed as

$$\lambda_v^2 = \lambda_{v1}^2 \cos^2\left(\frac{\pi}{4}\right) + \lambda_{v2}^2 \sin^2\left(\frac{\pi}{4}\right). \qquad \text{(D-1)}$$

Since $\lambda_{v1} = \lambda_{v2}$, the effective thermal conductivity of a vertical cell is simply denoted as λ_v'. Thus, eqn.(D-1) can be expressed as

$$\lambda_v^2 = \lambda_v'^2 \left(\cos^2\left(\frac{\pi}{4}\right) + \sin^2\left(\frac{\pi}{4}\right)\right) = \lambda_v'^2 . \qquad \text{(D-2)}$$

Therefore, the three figures are equivalent representations all having the same effective thermal conductivity λ_v.

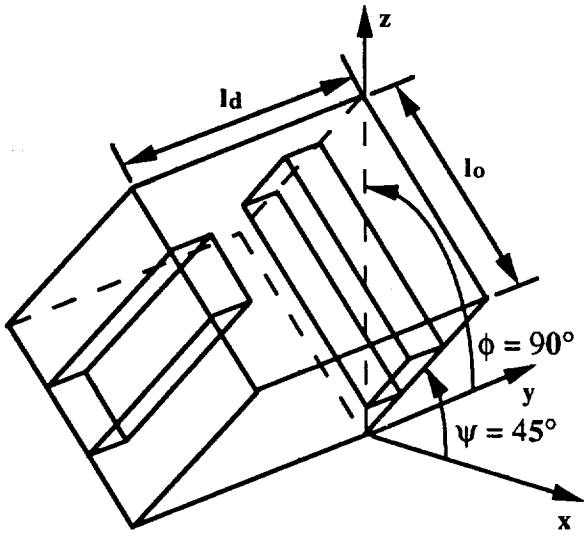

Figure D-1. Vertical cell rotated about the x-axis by 90° and rotated about the y-axis by 0°

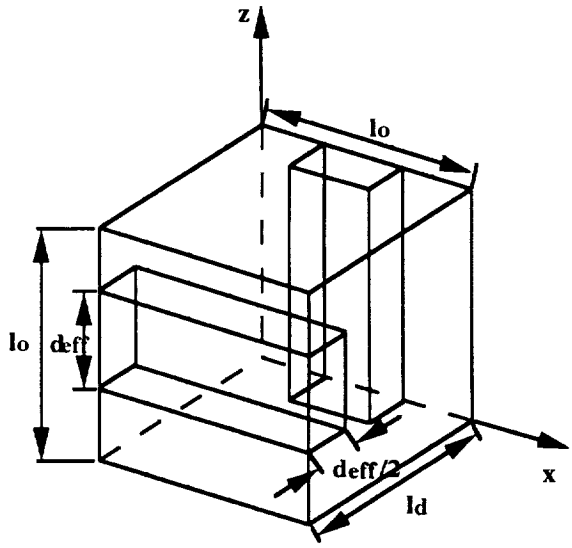

Figure D-2. Vertical cell rotated about the x-axis by 90° and rotated about the y-axis by 45°

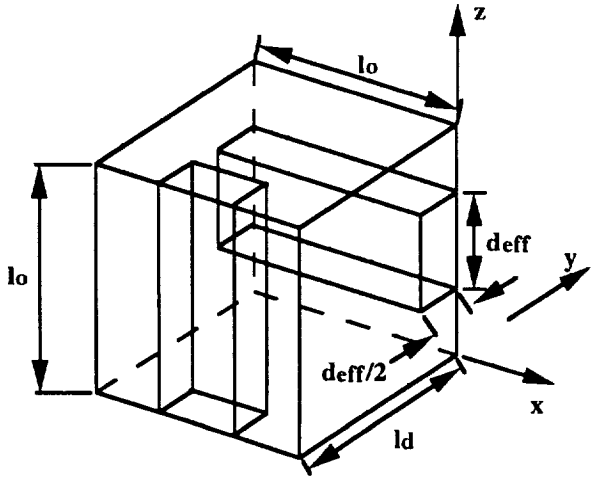

Figure D-3. Vertical cell rotated about the x-axis by 90° and rotated about the y-axis by -45°